


Article

Optimal Allocation of Hybrid Energy Storage System Based on Smoothing Wind Power Fluctuation and Improved Scenario Clustering Algorithm

Jinhua Zhang ^{1,*} , Tianyi Zhang ¹, Peng Cheng ¹, Dongzheng Yang ¹, Jie Yan ² and Xinpei Tian ¹

¹ School of Electrical Engineering, North China University of Water Resources and Electric Power, Zhengzhou 450045, China; ztyzhang1128@163.com (T.Z.); chengpeng@ncwu.edu.cn (P.C.); 17513364037@163.com (D.Y.); txp52629@126.com (X.T.)

² School of New Energy, North China Electric Power University, Beijing 102206, China; yanjie_freda@163.com

* Correspondence: zhangjh@ncwu.edu.cn

Abstract: Against the backdrop of the global energy transition, wind power generation has seen rapid development. However, the intermittent and fluctuating nature of wind power poses a challenge to the stability of grid operation. To solve this problem, a solution based on a hybrid energy storage system is proposed. The hybrid energy storage system is characterized by fast and precise control and bidirectional energy throughput, which can improve the impact of wind power fluctuations on grid stability. An ensemble empirical modal decomposition method was used to assign the raw wind power data to the grid-connected power and energy storage power commands with two reasonable corrections to meet the power allocation of the hybrid energy storage characteristics. In addition, a hybrid energy storage system model considering the whole life cycle cost was developed, and the optimal energy storage power cutoff was determined by exhaustively enumerating the high- and low-frequency power cutoffs. Finally, a comparison with a single storage capacity optimization model was carried out to verify the technical and economic advantages of hybrid energy storage in smoothing wind power fluctuations. To address the shortcomings of the traditional fuzzy c-means clustering algorithm, such as the need to specify the number of clusters in advance and sensitivity to the selection of the initial clustering centers, a combination of the cloud modeling theory and fuzzy c-means was used to make the process more automated and efficient. The improved clustering method algorithmic scheme had capacity error, power error, and cost error of around 3%, and the computational time was also significantly reduced and was computationally efficient compared to the full-year time series simulation. Through MATLAB (2020b) experimental simulation, it was found that the algorithm had a better balance of computational accuracy and efficiency.

Keywords: ensemble empirical mode decomposition; fuzzy control; second reasonable amendment; whole life cycle cost; cloud model; fuzzy c-means



Citation: Zhang, J.; Zhang, T.; Cheng, P.; Yang, D.; Yan, J.; Tian, X. Optimal Allocation of Hybrid Energy Storage System Based on Smoothing Wind Power Fluctuation and Improved Scenario Clustering Algorithm. *Processes* **2023**, *11*, 3407. <https://doi.org/10.3390/pr11123407>

Academic Editor: Michael C. Georgiadis

Received: 26 November 2023

Revised: 8 December 2023

Accepted: 8 December 2023

Published: 11 December 2023



Copyright: © 2023 by the authors. Licensee MDPI, Basel, Switzerland. This article is an open access article distributed under the terms and conditions of the Creative Commons Attribution (CC BY) license (<https://creativecommons.org/licenses/by/4.0/>).

1. Introduction

Wind energy has become an important source of energy in the global energy industry and plays a crucial role in meeting global energy demand. However, the gradual increase in the scale of wind power may result in the frequency of the power grid exceeding the limit value, which would seriously impair the safety and stability of power grid operation [1]. To maintain the safe and stable operation of the power system and balance power fluctuation between the load side and the power side, conventional generators must be started and stopped frequently and their load level must be reduced, which further reduces the operational efficiency and economy of the equipment in the power system [2].

Wind power energy storage not only saves energy but also improves the reliability of the grid and reduces the cost of electricity. Current energy storage technologies include pumped storage, superconducting energy storage, supercapacitors, electrochemical

batteries, flywheel energy storage, etc. [3]. Energy storage systems support the efficient connection of renewable energy sources to the smart grid, thereby facilitating the use of renewable energy sources on a larger scale while cost-effectively upgrading the existing grid infrastructure, thus potentially improving the economics [4,5]. A high-efficiency storage system (HESS) can have the advantages of both energy-based and power-based systems, break through the limitations of a single energy storage technology, and fully realize the transient and steady-state performance of the energy storage system [6]. Because hybrid energy storage systems can smooth out the fluctuations of wind power, their power signals have different frequency characteristics, and different energy carriers behave differently in terms of their frequency response to the power signals. Therefore, the study of power distribution in hybrid energy storage systems is an important factor in the realization of these systems. A rational power allocation strategy is a prerequisite for a HESS to utilize the complementary advantages of various energy storage components. Due to the declining cost and increasing popularity of lithium-ion batteries and the high efficiency and better sustainability of lithium-ion battery manufacturing [7], the authors of [8] used the source and sink model (SSM) to model Li-ion battery energy storage. SSM assumes that the storage voltage is constant and the power boundary is constant but ignores the chemical reaction and electrical characteristics of lithium batteries. In this regard, some researchers have tried to utilize the equivalent circuit model (ECM) to provide a more detailed portrayal of the energy storage characteristics and proposed a corresponding model construction method to match the ECM to the iterative optimization framework [9,10]. The authors of [11] used an improved low-pass filtering method to optimize the energy distribution of supercapacitors and lithium-ion batteries while solving the “overload” problem of conventional low-pass filtering methods. However, the algorithm suffers from a time lag. The authors of [12] studied an adaptive white noise filtering algorithm based on the Gaussian wavelet that automatically adjusts the level of wavelet decomposition according to the size of the output power change and achieves accurate division and power distribution within the frequency of the power signal. However, this requires sufficient historical data for reference.

All the methods outlined in the above studies can achieve effective decomposition and synthesis of wind signals; however, they cannot effectively handle nonlinear and nonsmooth signals. Due to the complexity of the spectral components of wind signals, it is difficult to detect them effectively using conventional detection algorithms. The basic functions of empirical modal decomposition (EMD) can be adaptively obtained from the input power signal and no longer need to be formulated in advance. Therefore, EMD can be better adapted to the characteristics of wind power signals. In [13], for the power allocation of hybrid energy storage systems, the EMD algorithm was used to cluster the high-frequency and low-frequency bands, and a capacity allocation model based on constrained stochastic fuzzy simulation was proposed. This method can smooth the fluctuation of wind power, effectively control the charging state, and ensure the stable operation of the energy storage system. With the application of EMD algorithms in HESS power allocation to address power fluctuations, improved noise-assisted EMD algorithms have also been proposed, including the ensemble empirical mode decomposition algorithm [14,15] and the complete set empirical mode decomposition algorithm with adaptive noise [16,17]. The authors of [18] proposed a coordinated control method for energy storage devices and DC bus when switching between on-grid and off-grid operation modes for microgrid systems and designed a power distribution second-order filtering control strategy that combined the energy storage metrics and the DC bus. A second-order filtering control strategy with power distribution was designed to control the corresponding converter in combination with the charging state of the energy storage device. A second-order filtering control strategy with power distribution was designed to control the operating state of the corresponding converter in conjunction with the charging state of the energy storage element.

The contradiction between how to coordinate the smoothing effect of wind power fluctuation and reduce the burden of energy storage device is one of the difficult hotspots in using energy storage to smooth wind power fluctuation. The authors of [19–21] used a

first-order low-pass filter to filter out the high-frequency fluctuation component of wind power so that the power injected into the grid becomes smooth. However, the selection of the filter time constant will affect the performance of the filter. The larger the time constant, the larger the fluctuation power will be, which will increase the cost of the energy storage device; if the time constant is too small, the power injected into the grid will not be smooth enough, resulting in failure to meet the requirements of grid connection. The authors of [22] employed a discrete Kalman filter based on fuzzy control to smooth the wind power output using the health state of the battery as a feedback quantity.

Currently, the improvement of optimization methods for energy storage capacity allocation involves two main aspects: objective optimization modeling and model optimization solution methods. When developing capacity allocation models, several factors must be considered, such as wind forecast errors, geographic variations, wind tracking and scheduling capabilities, and energy storage cycles. In [22], the uncertainty in wind energy forecasting was quantified and its analytical form obtained by introducing chance constraints. An energy storage capacity optimization model considering the wind energy forecast error was constructed, and a two-stage stochastic programming approach was used to solve the optimal energy storage capacity allocation scheme. In [23], in order to reduce the economic cost of rotating standby capacity and grid regulation for wind farms, a life-cycle cost model for energy storage systems was developed, and the system allocation scheme was optimized by maximizing the net profit. The authors of [24,25] used an improved particle swarm optimization (PSO) method to optimally configure the energy storage system to address the problems of the existing PSO method, such as the difficulty of solving and the tendency to fall into local extremes.

In [26], the maximum energy storage capacity each month was calculated; such data processing is bound to cause inefficiency in calculation. Using this method, the amount of data was significantly reduced, and the computational accuracy and efficiency were improved while maintaining the original data characteristics. The authors of [27] proposed to use Latin hypercube sampling with the fuzzy c-means algorithm to study the extraction and probability distribution of typical scenes and integrate it with the PSO algorithm to optimize the optimal solution. Compared to the traditional method, this method simplifies the iterative process, shortens the computation time, and improves the computational efficiency. However, it cannot reasonably determine the number of clusters and cannot avoid the randomness of the initial clustering center. In [28], a normalized PV energy storage system operating curve was used to reduce the 365-day annual energy storage curve to a typical operating curve. The normalization method of the cloud computing model improved the computational speed, but the accuracy of the capacity allocation result was low. Literature [29] in the capacity configuration of hybrid energy storage system, for the microgrid system of each energy storage unit for the optimal configuration of capacity, and in the process of considering the power fluctuations in grid-connected operation; to DC bus power fluctuations in the smallest and the various types of storage equipment optimal capacity ratio as the optimisation objective, and particle swarm algorithm is used to solve the problem.

The authors of [30] first used a filtering method to allocate power to the hybrid energy storage. They then added a power conditioning module to make the SOC of both closer to the optimal SOC and performed a secondary allocation based on the relevant metrics to minimize the difference with the original power. In [31], based on the initial allocation of hybrid energy storage power using a high-pass filter, hybrid energy storage charging and discharging rules based on the SOC of Li-ion batteries were established, and coordinated control of hybrid energy storage was achieved through overcharging and overdischarging protection and the maximum charging and discharging power limitation. The charge/discharge rule is simple, reliable, and easy to implement. However, it cannot accurately track the change of SOC in the long-term operation of the system or flexibly respond to possible extreme power demand. Therefore, fuzzy-logic-based control methods have also been introduced into the energy management of hybrid energy storage. The

authors of [32–35] all used hybrid energy storage SOC as the input parameter of fuzzy control and established fuzzy control rules to regulate the power command of hybrid energy storage through historical experience or empirical data in order to keep the energy storage SOC working in a reasonable range and avoid the phenomenon of overcharging and overdischarging. Compared to the method based on deterministic rules, the rule transition of fuzzy control in this method is realized through fuzzy rules and affiliation function, which makes the transition process more flexible and smoother with stronger logic.

In this study, for the output characteristics of wind power in wind power generation, EEMD decomposition was used to smooth out the wind power fluctuation. A two-stage allocation method applicable to hybrid energy storage power was used along with a capacity allocation method for the whole life cycle cost of the energy storage system, and a cloud-modeled improved fuzzy c-means clustering method was developed to deal with the year-round energy storage curve. The rest of the paper is structured as follows.

Section 2 details the EEMD decomposition method used for smoothing wind power fluctuations. The wind power data were decomposed into multi-IMFs and reconstructed to extract the grid-connected wind power and energy storage power. By studying the frequency response characteristics of batteries and supercapacitors, the primary power allocation of HESS was realized. Then, the uncertainty control was used to optimize the SOC of the energy storage system to complete the secondary power allocation of HESS. The simulation results showed that the two-stage allocation strategy improved the rationality of power allocation, and the EEMD decomposition method also had good generalization and superiority.

Section 3 describes the capacity allocation problem of a high-efficiency energy storage system (HESS), for which the lifetime of the battery and the optimal charging strategy were derived by adopting an event-oriented lifetime model and utilizing the rain flow counting method. The life cycle cost problem of HESS was also considered, where the life cycle cost of HESS was the optimization objective. Wind farm data were analyzed in detail by separating the high- and low-frequency bands, enumerating the various cutoff points to obtain the optimal key operating modes, and analyzing and comparing the costs of different hybrid energy storage methods. The economics of the algorithm was determined through simulations.

Section 4 outlines the results of wind power output. After the annual energy storage curves are obtained through EEMD decomposition processing, a cloud-model-based improved fuzzy c-means clustering method was used to extract and simplify the features of the annual energy storage curves. Eight types of typical operating curves were obtained to input into the hybrid energy storage system capacity optimization model. The results showed that this algorithm could automatically determine the number of clusters and the initial centers of clusters, avoiding unnecessary sensitivity errors and improving the stability and accuracy of the results.

2. Wind Power Signal Processing Based on Improved Empirical Mode Decomposition

Traditional control methods do not take into account the possible adverse effects of complex changes in wind power output scenarios on suppression control. The lack of adaptive control methods means it cannot be ensured that reliable grid-connected power can be obtained in the face of different wind power output scenarios. Likewise, the efficient and reasonable use of hybrid energy storage configuration capacity cannot be ensured [36]. To address the above problems, an EEMD decomposition method for smoothing wind power fluctuations is proposed in this study based on analyzing the amplitude frequency characteristics of the output power signal from wind farms and combining it with the technical regulations of wind power grid connection. This method is more robust and reliable than the EMD method and can analyze nonlinear and nonstationary signals more accurately. Then, according to the performance characteristics of battery–supercapacitor hybrid energy storage, a two-stage power allocation method is proposed to achieve a reasonable allocation of power commands within the hybrid energy storage system [37].

Finally, the optimal decomposition and reasonable allocation of wind power are verified from multiple angles through simulation experiments. The two-stage allocation strategy of energy storage power improves the reasonableness of the power allocation of the HESS. The EEMD decomposition method also has good universality and superiority.

2.1. Wind Power Decomposition and Reconstruction

The EEMD method is used to analyze nonlinear and unstable signals in wind power systems and is based on EMD with random perturbations added to solve the problems of modal mixing and slow convergence in EMD. Unlike traditional Fourier analysis, EEMD is an adaptive signal processing method. The essence of the method is to repeatedly sieve and decompose the complex input signals according to their characteristics to obtain a series of IMFs with different frequencies. The specific wind power data decomposition steps for EEMD are as follows:

- (1) Assume that wind power data decomposition needs to be performed k times.
- (2) Extract the original wind power signal $P_W(t)$ and add white noise $n_i(t)$ to obtain $P_{W,i}(t)$, which is $P_{W,i}(t) = P_W(t) + n_i(t)$.
- (3) Calculate the upper and lower envelopes of a new series of raw signals $P_{W,i}(t)$ and calculate their mean values $m_{1,i}(t)$.
- (4) Calculate the first-order component $h_{1,i}(t)$, which is the difference between the raw wind power data $P_{W,i}(t)$ and the mean value $m_{1,i}(t)$.

$$h_{1,i}(t) = P_{W,i}(t) - m_{1,i}(t) \quad (1)$$

- (5) Judge whether $h_{1,i}(t)$ satisfies the condition of IMF. If it satisfies it, take it as the first-order IMF high-frequency component $c_{1,i}(t)$; otherwise, take $h_{1,i}(t)$ as the new $P_{W,i}(t)$. Repeat steps 4 and 5 in a loop until $h_{1,i}(t)$ that satisfies the IMF condition is obtained.

$$c_{1,i}(t) = h_{1,i}(t) \quad (2)$$

- (6) Find the difference between the original signal and the first-order IMF component $r_{1,i}(t)$.

$$r_{1,i}(t) = P_{W,i}(t) - c_{1,i}(t) \quad (3)$$

- (7) Repeat steps 3 to 5 in a loop using $r_{1,i}(t)$ as the new signal $x_i(t)$ until the value of p -order $c_{p,i}(t)$ obtained is constant or monotonic, at which point $c_{p,i}(t)$ is the residual component obtained from the decomposition.

$$\begin{cases} r_{1,i}(t) - c_{2,i}(t) = r_{2,i}(t) \\ \vdots \\ r_{p-1,i}(t) - c_{p,i}(t) = r_{p,i}(t) \end{cases} \quad (4)$$

The original signal can be expressed as a superposition of several IMF components and a residual component after EEMD decomposition. By analyzing the IMF components obtained from the decomposition, the fluctuation characteristics on different scales can be obtained, and the stability and predictability of wind power can be studied.

$$P_{W,i}(t) = \sum_{m=1}^p c_{p,i}(t) + r_{p,i}(t) \quad (5)$$

- (8) Repeat steps 2 to 7 for k times.
- (9) Find the mean value of the IMF of each order to obtain $a_p(t) = \frac{1}{k} \sum_{i=1}^k a_{i,p}(t)$, which is the result of EEMD decomposition.

The flowchart of the decomposition steps is shown in Figure 1 below:

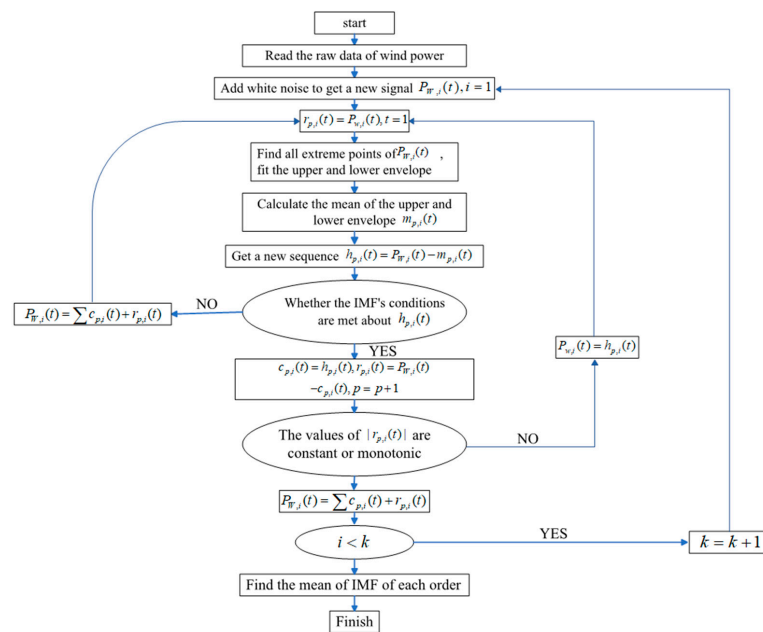


Figure 1. EEMD wind power decomposition flow chart.

Figure 2 below shows the power amplitude of each IMF with the corresponding frequency value. It can be seen that the amplitude of IMF3 is higher, the frequency is lower, and the oscillation is smoother. It is representative of the original wind signal oscillation, and it is the low-frequency band of the reconstructed signal. While the amplitude of the IMF1 signal is the lowest, the instantaneous frequency is the highest. The frequency of the movement is also the highest, and the high-frequency component of the IMF1 signal is the highest frequency component of the reconstructed signal.

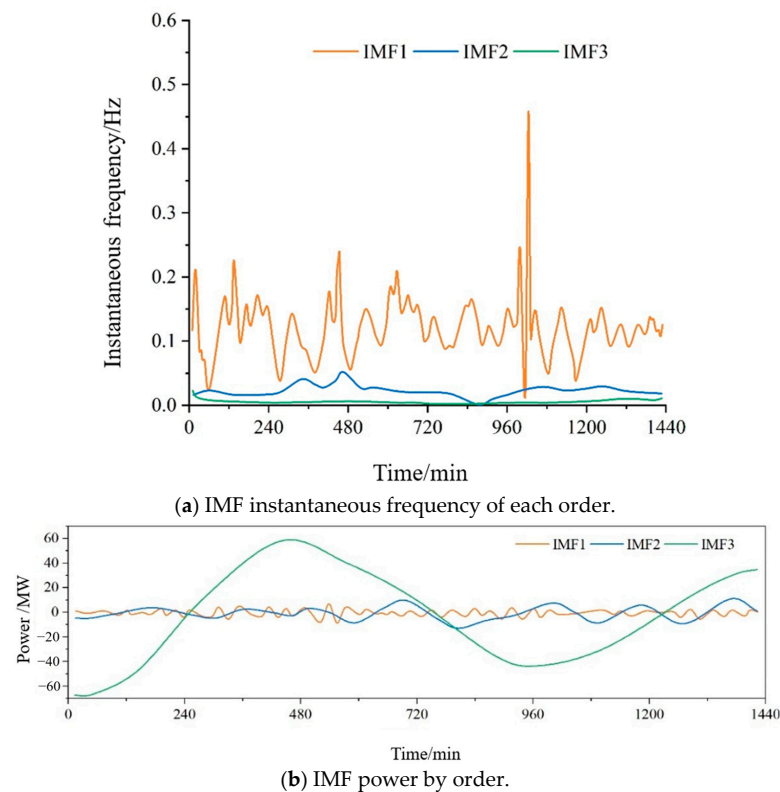


Figure 2. IMF's amplitude and frequency curves.

Combined with the wind power fluctuation range, each IMF component is reconstructed and categorized as a low-frequency component if its frequency is lower than the limit or as a high-frequency component if its frequency is greater than the frequency of the limit. Because the original signal is the sum of the IMF components of each line obtained by decomposition, the IMF reconstruction is computed by superimposing a certain index of high- and low-frequency band components to obtain the low- and high-frequency components [38].

Here, the reconstruction method is divided into high-frequency reconstruction $f2c$ and low-frequency reconstruction $c2f$. The high-frequency reconstruction generates the high-frequency reconstruction components of each order according to the top-down superposition of the EEMD decomposition results: $f2c(1)$ is IMF1, $f2c(2)$ is IMF1 + IMF2, and $f2c(p + 1)$ is $IMF1 + IMF2 + \dots + IMFp + res$, where p is the total number of orders of the IMF, and the specific reconstruction method is shown in Equation (6).

$$\begin{aligned} f2c(1) &= IMF1 \\ f2c(2) &= IMF1 + IMF2 \\ &\dots \\ f2c(p + 1) &= IMF1 + IMF2 + \dots + IMFp + res \end{aligned} \quad (6)$$

The low-frequency reconstruction generates the low-frequency reconstruction components of each order according to the bottom-up superposition of the EEMD decomposition results: $c2f(1)$ is res , $c2f(2)$ is $res + IMFp$, $c2f(p + 1)$ and $res + IMFp + \dots + IMF1$ is $IMF1 + IMF2 + \dots + IMFp + res$, where p is the total number of IMF orders, and the specific reconstruction is shown in Equation (7).

$$\begin{aligned} c2f(1) &= res \\ c2f(2) &= res + IMFp \\ &\vdots \\ c2f(p + 1) &= res + IMFp + \dots + IMF1 \end{aligned} \quad (7)$$

One of the key elements to realize the stable operation of the power system is how to extract the grid-connected part effectively from the power data to meet the requirements of not only the power grid but also the hybrid energy storage system. In order to solve this problem, this study adopted the EEMD method to decompose the original signal to determine the direct grid-connected component, used the corresponding high-frequency reconstruction component as a hybrid energy storage power task, and combined the variance constraints of grid-connected wind power to reconstruct the decomposed IMF so as to adapt to the fluctuations of different time scales and better cope with the time variability and instability of wind power signals. Taking a typical day as an example, EEMD decomposition was performed to obtain each order component, and the decomposition results are shown in Figure 3.

As can be seen from the Figure 3 above, the original wind power signal was decomposed into sum. The high- and low-frequency reconstruction methods were carried out, and the obtained levels were decomposed and reconstructed. Figure 4 shows the reconstruction results at low frequency, and Figure 5 shows the reconstruction results at high frequency.

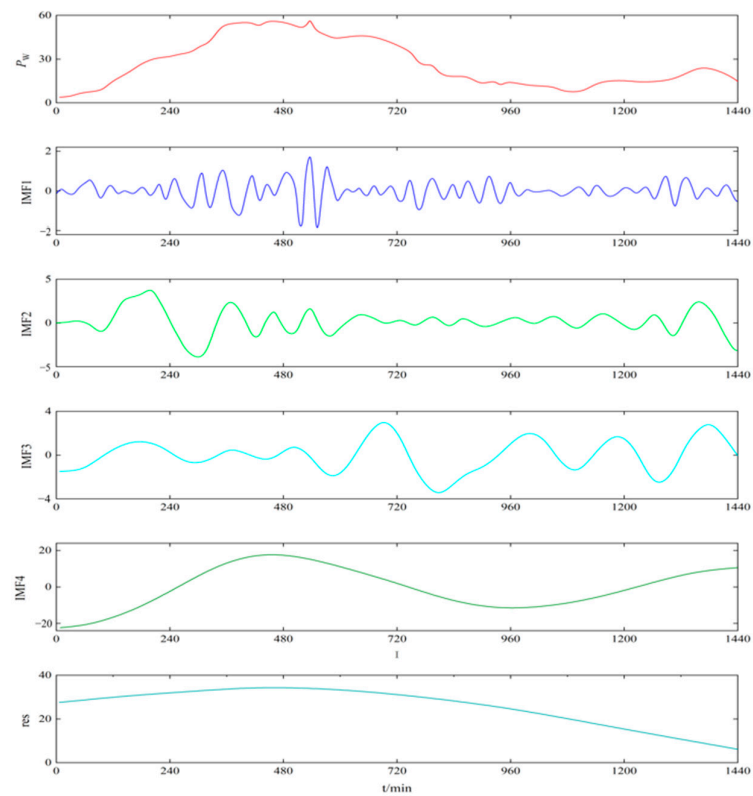


Figure 3. EEMD decomposition results.

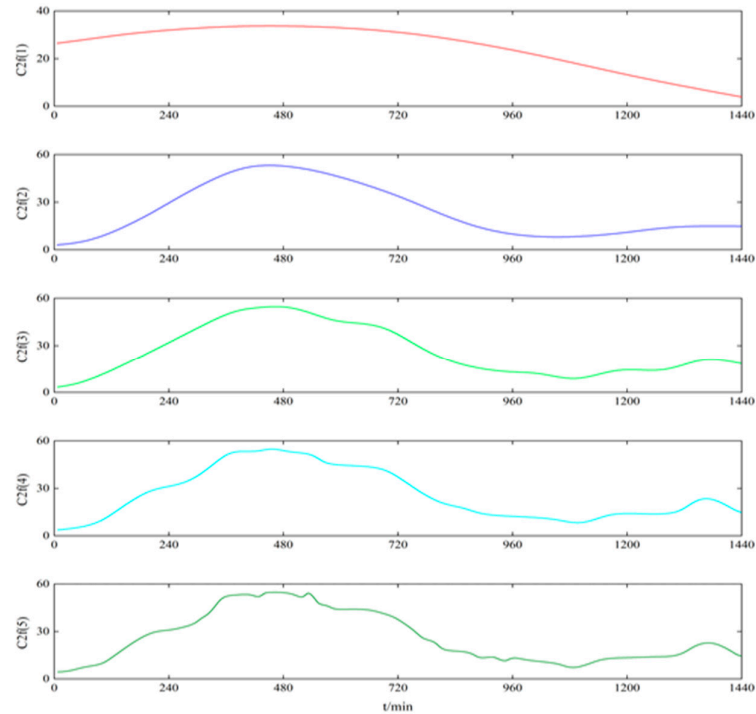


Figure 4. Low-frequency reconfiguration.

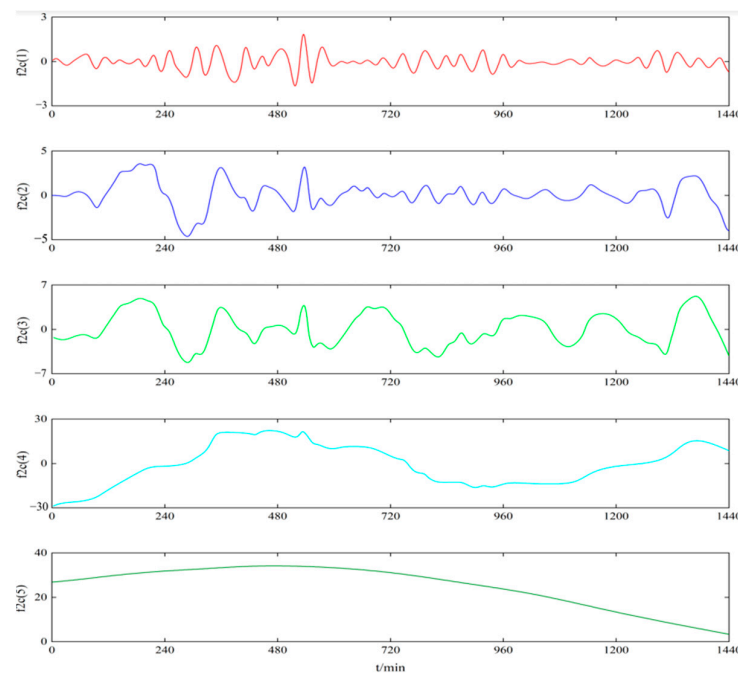


Figure 5. High-frequency reconfiguration.

Figure 6 shows the calculation results. As can be seen from the Figure 6, the maximum wave momentum of the low-frequency reconstructed component gradually increased with the increase in the order of the component, and the maximum wave momentum of the low-frequency reconstructed component was greater than the grid-connected fluctuation limit. Therefore, $\text{res} + \text{IMF4} + \text{IMF3} + \text{IMF2}$ was selected as the grid-connected component. $\text{F2c}(1)$, that is, IMF1 , was selected as the hybrid energy storage task.

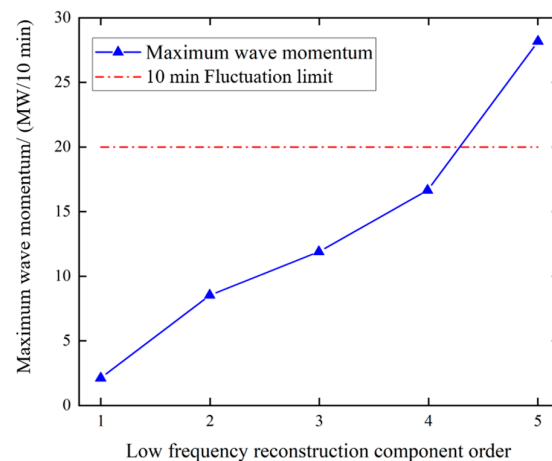


Figure 6. Grid-connected component screening.

2.2. Adaptation to Different Typical Wind Power Scenarios

Taking a 60 MW wind farm as an example, three typical cases of wind power output power $P_{w1}(t)$, $P_{w2}(t)$, and $P_{w3}(t)$ of this wind farm were modeled and simulated to verify the generality of the EEMD decomposition method for different wind power cases. The EEMD adaptivity was utilized to obtain the component order 2 that satisfied the grid-connected fluctuation criterion as well as the grid-connected powers $P_{o1}(t)$, $P_{o2}(t)$, and $P_{o3}(t)$, respectively, as shown in Figure 7. The order P_{o1} of scenario 1 was 4; the order P_{o2} of scenario 2 was 3, which is relatively gentle; and the order P_{o3} of scenario 3 was 5, which is more intense. The order of the low-frequency reconstruction components changed

according to the fluctuation characteristics of wind power in different scenarios, and the extracted grid-connected power met the fluctuation criteria.

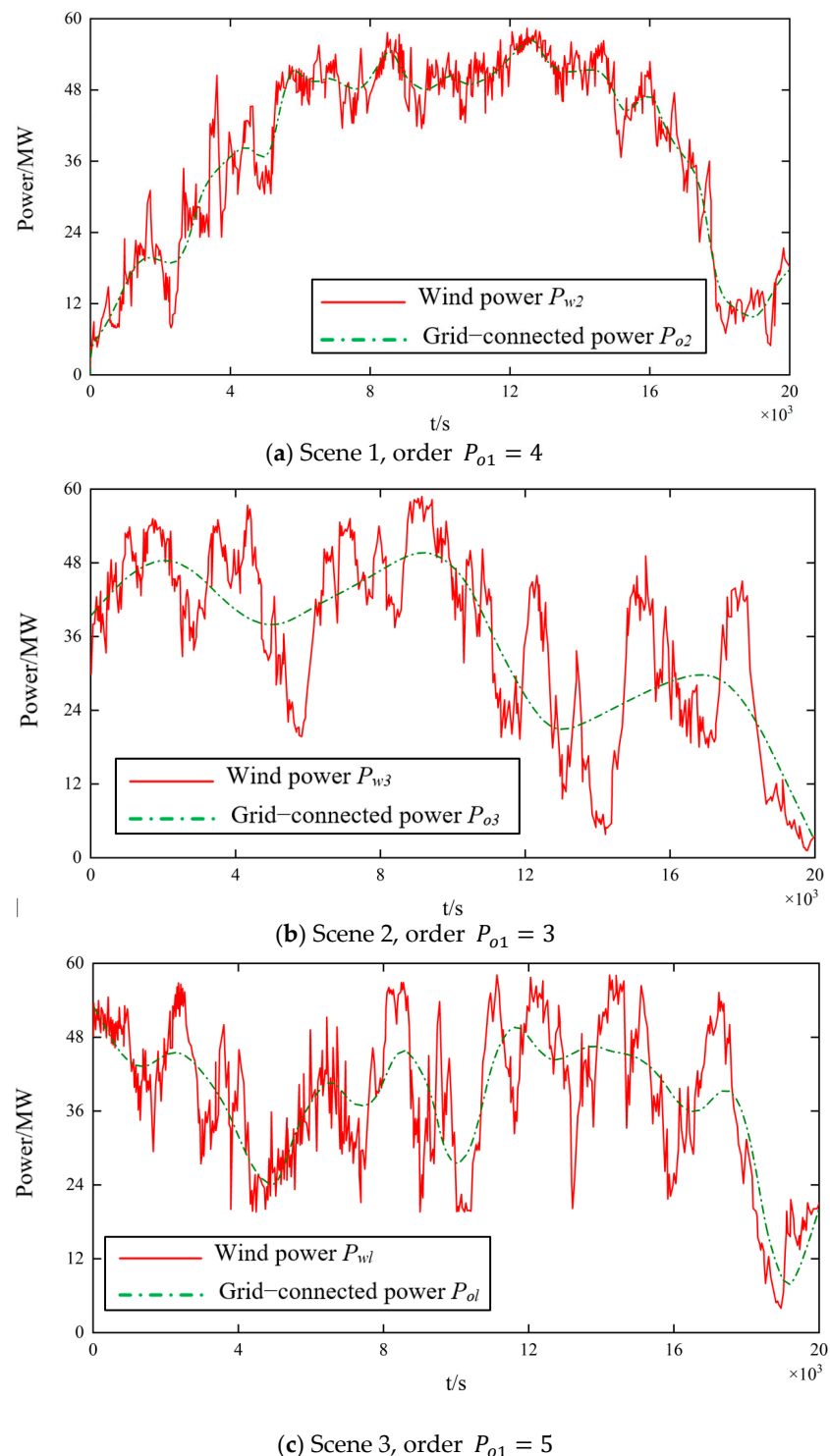


Figure 7. Different scene decomposition effect.

2.3. Analysis of Wind Power Flattening Effect

In order to study the smoothing effect of EEMD decomposition on the electrical system, the electrical system was smoothed by EEMD decomposition and compared with the low-pass filtering method in the same case.

As can be seen from Figure 8, compared to the low-pass filtering algorithm, the grid-connected power obtained by the EEMD decomposition algorithm was more stable. Both

algorithms generated a large amount of peak power based on the original power change and reduced the cumulative power change. However, the EEMD decomposition algorithm achieved greater reduction, better smoothing effect, and superiority.

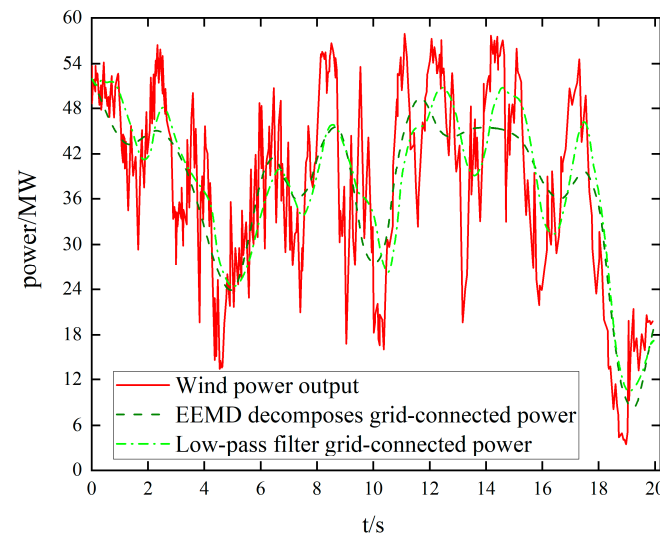


Figure 8. Different algorithm leveling effect.

2.4. Analysis of the Effect of Secondary Fuzzy Correction

The initial power command assignment is made only from the response frequency characteristics of Li-ion batteries and supercapacitors and is assigned by controlling the charge/discharge response frequency of Li-ion battery storage to achieve extended battery life cycle. In practice, hybrid energy storage systems must consider limitations such as the state of charge (SOC) and charge/discharge responsiveness of the storage device. Ultracapacitor energy storage devices with low energy density are more susceptible to overcharge/discharge and insufficient responsiveness. Therefore, in this study, a quadratic correction of the hybrid energy storage internal power command allocation was considered according to the hybrid energy storage SOC state to ensure that the state of charge is always within a safe range. Separate and independent fuzzy controllers were used to carry out the secondary correction for Li-ion batteries and supercapacitors to further optimize their energy storage power command allocation. In this process, the state of charge (SOC) of the energy storage is an important indicator of the charging and discharging capability of the energy storage, which indicates the percentage of the remaining power to the rated capacity. By optimizing the SOC, we can better control the charging and discharging process of the hybrid energy storage system and ensure that the energy storage system is able to maintain optimal performance in a variety of real-world situations.

The energy storage charging state $SOC(t)$ with remaining capacity $E(t)$ and rated capacity E_{Ah} at time t is expressed as follows:

$$SOC(t) = E(t)/E_{Ah} \quad (8)$$

The stored energy during charging and discharging was calculated using the ampere–time integration method:

$$SOC(t) = (1 - \sigma_{sdr})SOC(t-1) + P(t)\Delta t\eta_c \quad (9)$$

$$SOC(t) = (1 - \sigma_{sdr})SOC(t-1) - \frac{P(t)\Delta t}{\eta_d} \quad (10)$$

where $P(t)$ is the charging and discharging power of the energy storage; σ_{sdr} is the self-discharge rate; η_c and η_d are the charging and discharging efficiencies, respectively; and Δt is the sampling time interval.

The charging and discharging model of the energy storage system and the calculation model of SOC were established, and the charging states $SOC_b(t)$ and $SOC_{sc}(t)$ of the lithium battery and supercapacitor were introduced into the independent fuzzy controllers to optimize the initial power of the energy storage system to ensure that the charging states are always within the safety range. The fuzzy rules for lithium battery are as follows:

- (1) When the Li-ion battery $SOC_b(t)$ is at a reasonable level, it can be charged and discharged according to the original initial allocation of power instructions without further optimization.
- (2) When $SOC_b(t)$ is small, it indicates that the lithium-ion battery storage energy is in an undercapacity state. If the energy storage is in the discharging state $P_b(t) < 0$ at this time, $P_b(t)$ is corrected to make it larger; if the energy storage is in the charging state $P_b(t) > 0$ at this time, no correction is made.
- (3) If $SOC_b(t)$ is larger, it means that the storage capacity of the battery may be approaching saturation, i.e., the battery is nearing its maximum capacity and needs to be discharged. If it is then in the charging state, i.e., $P_b(t) > 0$ means that a correction $P_b(t)$ is necessary to reduce the storage capacity; if when in the discharging state, i.e., $P_b(t) < 0$, and the energy is sufficient at this time, there is no need for a correction.

The charging and discharging power of lithium batteries and ultracapacitors is corrected for

$$\begin{aligned} P_b^*(t) &= P_b(t) + \Delta P_b(t) \\ P_{sc}^*(t) &= P_{sc}(t) + \Delta P_{sc}(t) \end{aligned} \quad (11)$$

where $P_b^*(t)$ and $P_{sc}^*(t)$ are the corrected lithium battery and supercapacitor charging and discharging power at time t , respectively; $\Delta P_b(t)$ and $\Delta P_{sc}(t)$ are the corrected power of Li-ion battery and supercapacitor at time t , respectively.

In this study, a dual-input single-output fuzzy controller was used, with the state of charge of Li-ion batteries and supercapacitors as input one and a trapezoidal affiliation function, whose domain was $[0, 1]$. The moderate, smaller, and larger states of the above state of charge were materialized as fuzzy sets $\{NB, NM, NS, ZO, PS, PM, PB\}$, denoting $SOC_b(t)$ and $SOC_{sc}(t)$ {very low, low, lower, moderate, higher, higher, and very high}; normalized $P_b(t)$ and $P_{sc}(t)$ were used as inputs two, and a trigonometric affiliation function was chosen, whose domain was $[0, 1]$. The fuzzy set was $[D, C]$, denoting {discharge, charge}, respectively; the modified power $\Delta P_b(t)$ and $\Delta P_{sc}(t)$ were used as outputs. The fuzzy control rules of lithium battery and supercapacitor are shown in Table 1, and the input and output affiliation functions of lithium battery are shown in Figure 9. The supercapacitor fuzzy controller and lithium battery fuzzy rules are similar, so this paper will not repeat the discussion.

Table 1. Fuzzy control rules for lithium batteries.

$\Delta P_b(t)/\Delta P_{sc}(t)$		$SOC_b(t)/SOC_{sc}(t)$						
		NB	NM	NS	ZO	PS	PM	PB
$P_b(t)/P_{sc}(t)$	D	PB	PM	PS	ZO	ZO	ZO	ZO
	C	ZO	ZO	ZO	ZO	NS	NM	NB

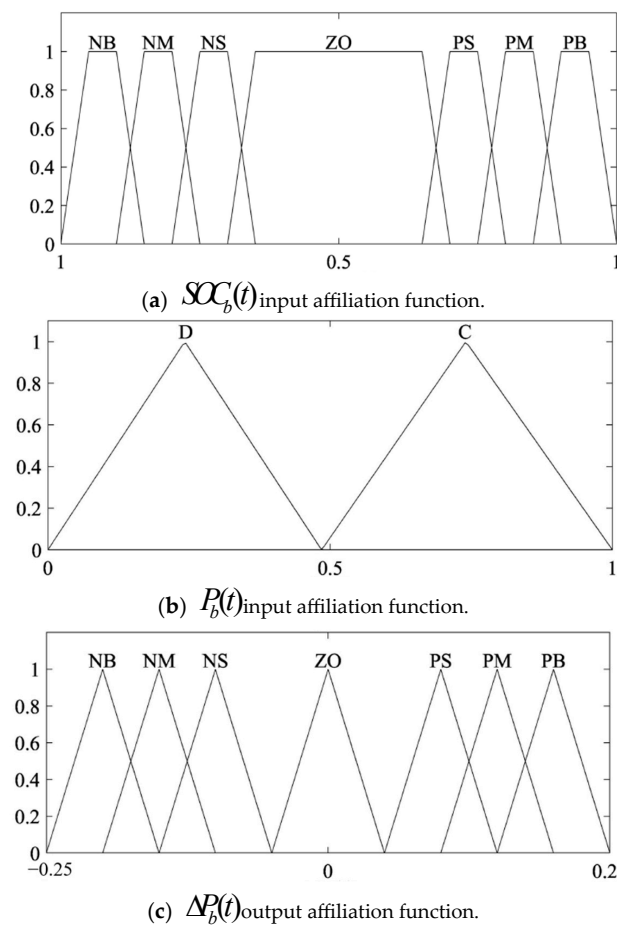


Figure 9. Lithium battery input and output affiliation functions.

The set charge/discharge efficiencies were 90% and 95% for lithium batteries and ultracapacitors, respectively. Independent fuzzy control was used to correct the power distribution of lithium battery and supercapacitor twice to ensure the power balance between the two groups. Figure 10 shows the comparison of lithium battery and supercapacitor before and after fuzzy control optimization. The comparison of charge and discharge power instructions for the secondary distribution of the lithium battery and supercapacitor after fuzzy control correction is shown in Figure 11.

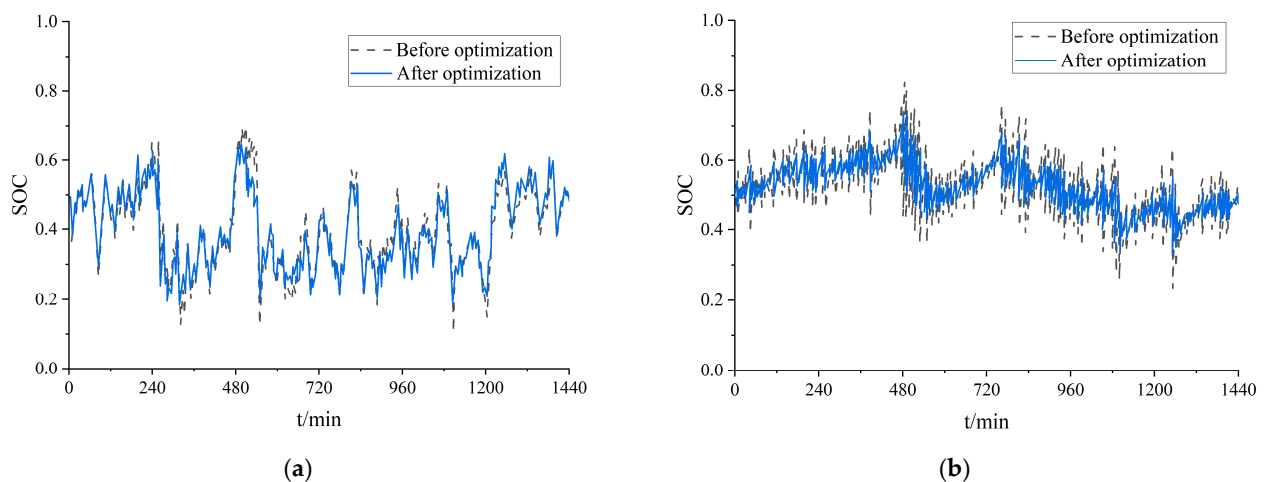


Figure 10. SOC curve before and after secondary optimization: (a) SOC curve comparison of lithium batteries; (b) comparison of ultracapacitor SOC curves.

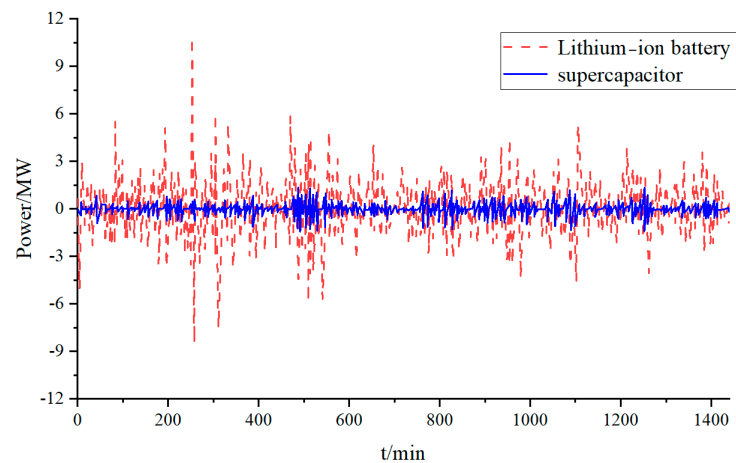


Figure 11. Hybrid energy storage power secondary distribution.

The changes in the lithium-ion battery and the supercapacitor before and after the optimization of fuzzy control were analyzed and compared. The results showed that the use of the fuzzy controller achieved maximum of 71% to 63% and minimum of 10% to 21% for the lithium-ion battery and maximum of 84% to 73% and minimum of 22% to 33% for the supercapacitor. By comparing these two schemes, it can be concluded that the optimized scheme was in the reasonable range. In future work, different fuzzy control rules for charging and discharging energy storage devices can be formulated to reduce the destructive effects of overcharging and overdischarging on the performance of energy storage devices.

Through the initial allocation based on charge and discharge response time division of energy storage and the secondary correction of fuzzy control based on hybrid energy storage SOC, reasonable allocation of hybrid energy storage power commands was realized, and the control stability and operation economy of the hybrid energy storage system were ensured.

3. Hybrid Energy Storage Capacity Allocation Based on Whole-Life Costs

Hybrid energy storage systems can make use of the advantages of lithium battery and supercapacitor energy storage to complement each other and better adapt to the complex fluctuations of wind power generation. The structure of the combined wind storage system is shown in Figure 12, in which lithium batteries and supercapacitors are connected to the grid-connected bus after power conversion through mutually independent converters. When using the energy storage system with wind power generation, wind power generation unit output access to the AC bus for smoothing control and then connected to the grid, suitable for large and medium-sized wind farms output power fluctuation smoothing control. Lithium batteries can handle the low-frequency part of wind power fluctuation and provide long-time power regulation; supercapacitors can handle the high-frequency fluctuation part and prolong the service life of lithium batteries. However, the cost of the supercapacitor is high, and its introduction may reduce the overall economy of the energy storage system. Therefore, to satisfy the wind balance demand while minimizing the system cost, the power and capacity of hybrid energy storage need to be configured appropriately. In this study, an event-oriented life quantification model was used to determine the relationship between the charge/discharge state and battery life under different power commands and compare the annual integrated cost of hybrid energy storage systems.

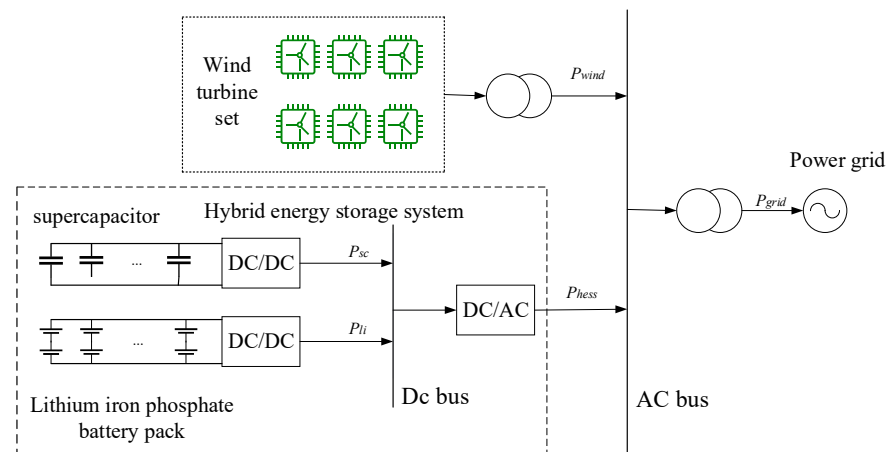


Figure 12. Wind storage combined system structure.

3.1. Energy Storage System Capacity Allocation Model

3.1.1. Lithium Battery Capacity Configuration Model

According to the previous analysis of energy storage selection, the type of storage battery selected was lithium iron phosphate battery, which has high energy density, long working time, and low cost and can effectively undertake the work of smoothing the main low-frequency components of wind power fluctuations [39]. The annual average cost C_B of lithium battery energy storage systems basically includes the value of initial investment cost C_{B1} and annual operation and maintenance cost C_{B2} . The initial investment cost is the initial investment, which is determined by the rated power and rated capacity. Initial investment cost C_{B1} is the initial investment, which is determined by the rated power P_B and rated capacity E_B . The power part reflects the value of the energy storage energy conversion system, while the capacity part refers to the value of the energy storage equipment itself. The initial investment cost C_{B1} can be expressed by the equal annual value method as follows:

$$C_{B1} = (aP_B + bE_B) \frac{r_0(1 + r_0)^{T_b}}{(1 + r_0)^{T_b} - 1} \quad (12)$$

where a , b , and T_b are the power cost factor, capacity cost factor, and operating life of the lithium battery, respectively, and r_0 is the discount rate.

The annual operation and maintenance cost C_{B2} is determined by the rated capacity E_B and rated power P_B :

$$C_{B2} = mP_B + nE_B \quad (13)$$

where m and n are the power and capacity operation and maintenance cost factors of lithium batteries. The optimization objective of the wind farm side energy storage system is to reasonably allocate the storage power and power level to minimize the annual comprehensive cost of the energy storage system under the premise of meeting the standard of fluctuation smoothing and power level so that the annual comprehensive cost of the energy storage system is minimized. The objective function for the optimal allocation of the capacity of a lithium battery storage system is to minimize the average annual integrated cost C_B :

$$\min f_B = C_B = C_{B1} + C_{B2} = (aP_B + bE_B) \frac{r_0(1 + r_0)^{T_b}}{(1 + r_0)^{T_b} - 1} + mP_B + nE_B \quad (14)$$

The following SOC constraints, charge/discharge responsiveness constraints, and energy conservation constraints were considered:

- (1) SOC constraint: the state of charge of Li-ion battery should be within the following limit:

$$SOC_{bmin} \leq SOC_b(t) \leq SOC_{bmax} \quad (15)$$

where the charging state for safe operation is between SOC_{bmax} and SOC_{bmin} .

- (2) Charge/discharge responsiveness constraint: lithium battery power corresponds to the charge/discharge power constraint as follows:

$$\max(-P_B, \frac{E_b(t) - E_B}{\Delta t \eta_{Bc}}) \leq P_b(t) \leq \min(P_B, \frac{E_b(t) - E_B}{\Delta t} \eta_{Bd}) \quad (16)$$

where $E_b(t)$ is the battery residual capacity at time t , η_{Bc} and η_{Bd} are the charging and discharging efficiencies of the lithium battery, and Δt is the sampling interval time.

- (3) Energy conservation constraints: wind power output is equal to the battery storage power command and the sum of grid-connected power; the battery from the outside world absorbs and releases the energy conservation as follows:

$$\begin{aligned} P_b(t) + P_o(t) &= P_w(t) \\ \sum_{t=1}^T P_b(t) &= 0 \end{aligned} \quad (17)$$

where $P_b(t)$ is the charging and discharging power of the lithium battery at time t .

3.1.2. Supercapacitor Energy Storage Capacity Allocation Model

The annual average integrated cost of supercapacitor C_{SC} mainly includes the annual value of the initial investment cost C_{SC1} and the annual operation and maintenance cost C_{SC2} . The objective is to minimize the annual average integrated cost C_{SC} . The model is based on the following:

$$\min f_{SC} = C_{SC} = C_{SC1} + C_{SC2} = (cP_{SC} + dE_{SC}) \frac{r_o(1+r_o)^{T_{SC}}}{(1+r_o)^{T_{SC}} - 1} + xP_{SC} + yE_{SC} \quad (18)$$

where P_{SC} and E_{SC} are the rated power and rated capacity of the supercapacitor MW, respectively; c , d , x , and y are the power cost coefficient, power O&M cost coefficient, capacity cost coefficient, and capacity O&M cost coefficient of the supercapacitor, respectively; and T_{SC} is the operating life of the supercapacitor.

The SOC, charge/discharge responsiveness, and energy conservation are constrained as follows:

$$\begin{aligned} SOC_{SCmin} &\leq SOC_{SC}(t) \leq SOC_{SCmax} \\ \max(-P_{SC}, \frac{E_{SC}(t) - E_{SC}}{\Delta t \eta_{SCc}}) &\leq P_{SC}(t) \leq \min(P_{SC}, \frac{E_{SC}(t) - E_{SC}}{\Delta t} \eta_{SCd}) \\ P_{SC}(t) + P_o(t) &= P_w(t) \\ \sum_{t=1}^T P_{SC}(t) &= 0 \end{aligned} \quad (19)$$

where $P_{SC}(t)$ is the charging and discharging power of the supercapacitor at time t ; $SOC_{SC}(t)$ is the charging state at time t ; the range of safe operation charging state is between SOC_{SCmax} and SOC_{SCmin} ; $E_{SC}(t)$ is the remaining power at time t ; η_{SCc} and η_{SCd} are the charging efficiency and discharging efficiency, respectively.

3.1.3. Hybrid Energy Storage Capacity Allocation Model

Although the energy storage power extracted from wind energy can be used as a control index for individual energy storage units, to achieve the goal of stable and reliable operation of the system, it is necessary to effectively divide and control the energy distribution of each energy storage system unit and to reasonably configure the energy storage components and power distribution.

If the threshold is too low, the “over-smoothing” component of the high-frequency power control of the supercapacitor will lead to prolonged discharge time and insufficient

storage capacity, which in turn will lead to an increased demand for storage capacity and higher system investment costs. If the threshold is too high, the number of components in the low-frequency power control of lithium-ion batteries will increase, which will accelerate the degradation of battery life and lead to higher system costs. By combining the power control distribution of the hybrid energy storage system with the overall cost of the energy storage system and comparing it with the economic cost of the energy storage system under different cutoff points, a reasonable power control distribution of the energy storage can be realized, the optimal power control cutoff point can be determined, and then the hybrid energy storage configuration system with the lowest economic cost can be determined, which can improve the performance and reliability of the hybrid energy storage system.

The objective function of the hybrid energy storage system capacity allocation model is as follows:

$$\min f = C_B^* + C_{SC}^* \quad (20)$$

where

$$\begin{aligned} C_B^* &= C_{B1} + C_{B2} + C_{B3} = \\ &(aP_B + bE_B) \frac{r_0(1+r_0)^{T_b}}{(1+r_0)^{T_b}-1} + mP_B + nE_B + \\ &\sum_{i=1}^n (k_{pg}P_B + bE_B)(1+r_0)^{\frac{iT_b}{n+1}} \end{aligned} \quad (21)$$

$$C_{SC}^* = C_{SC} + C_{SC} = (cP_{SCt} + dE_{SCy}) \frac{r_0(1+r_0)^{T_{SC}}}{(1+r_0)^{T_{SC}}-1} + xP_{SC} + yE_{SC} \quad (22)$$

where C_B^* and C_{SC}^* were the annual integrated cost of lithium battery storage and supercapacitor energy storage, respectively; C_{B3} and k_{pg} are the lithium battery renewal replacement cost and other annual values and power update cost coefficients, respectively; f is the annual integrated cost of the hybrid energy storage system; and n is the number of lithium battery renewal replacements.

The SOC constraints of charge/discharge response and energy conservation constraints are as follows:

$$\begin{aligned} \max(-P_{sc}, \frac{E_{sc}(t)-E_{sc}}{\Delta t \eta_{sc}}) &\leq P_{sc}(t) \leq \min(P_{sc}, \frac{E_{sc}(t)-E_{sc}}{\Delta t} \eta_{scd}) \\ \max(-P_B, \frac{E_b(t)-E_B}{\Delta t \eta_{BC}}) &\leq P_b(t) \leq \min(P_B, \frac{E_b(t)-E_B}{\Delta t} \eta_{Bd}) \end{aligned} \quad (23)$$

$$\begin{aligned} SOC_{scmin} &\leq SOC_{sc}(t) \leq SOC_{scmax} \\ SOC_{bmin} &\leq SOC_b(t) \leq SOC_{bmax} \end{aligned} \quad (24)$$

$$\begin{aligned} P_b(t) + P_{sc}(t) + P_o(t) &= P_w(t) \\ \sum_{t=1}^T P_h(t) &= 0 \end{aligned} \quad (25)$$

Considering the overall energy distribution and total cost, the economic cost of the hybrid energy storage system at each boundary point is usually analyzed, and the hybrid energy storage system with the highest economic cost is preferred. Based on the above study, the objective of this project was to analyze the economic performance of the hybrid energy storage system under different boundary point conditions and optimize its configuration to improve its overall performance and reliability.

3.2. Determination of the Optimal Critical Point

Taking a 60 MW wind farm as an example, the above single energy storage and hybrid energy storage capacity allocation models were applied to optimize the capacity of the energy storage system for smoothing wind power fluctuations. Considering the wind power curve of the wind farm on a certain day, the grid-connected1 and the storage power2 curves obtained from EEMD decomposition were selected, as shown in Figure 13. The relevant economic and technical parameters of the hybrid energy storage system are shown in Table 2 [20], where the lifetime of the supercapacitor energy storage is fixed at 20 years,

thus focusing on the impact of battery lifetime changes on the system configuration results.

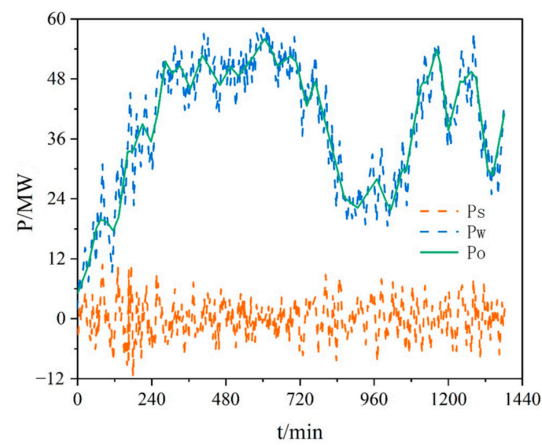


Figure 13. Typical daily power curve.

Table 2. Energy storage system coefficient. Reproduced with permission from [20].

Type of Energy Storage	Li-Ion Battery	Supercapacitor
Cost		
Cost per unit of power/RMB KW ⁻¹	9300	1800
Unit capacity cost/RMB KW ⁻¹	9300	12,400
Renewal cost per unit of power/RMB KW ⁻¹	2472	1860
Unit capacity renewal cost/RMB KW ⁻¹	9300	12,400
Auxiliary cost per unit of power/RMB KW ⁻¹	620	620
Ancillary cost per unit of capacity/RMB KW ⁻¹	0	0
O&M cost per unit of power/RMB KW ⁻¹	155	80.6
O&M cost per unit of capacity/RMB KW ⁻¹	0.014	0.0134
Cost of end-of-life disposal/RMB KW ⁻¹	465	93
Life cycle/times	4000	20 years
Charge and discharge efficiency	0.85	0.95
SOC upper and lower limits	[0.2, 0.8]	[0.1, 0.95]

In this study, the primary power distribution was adopted, and the power distribution scheme under different critical modes was calculated using the exhaustive method, which was substituted into the life cycle model of the hybrid energy storage system, as shown in Figure 14. The corresponding annual comprehensive cost was subsequently calculated.

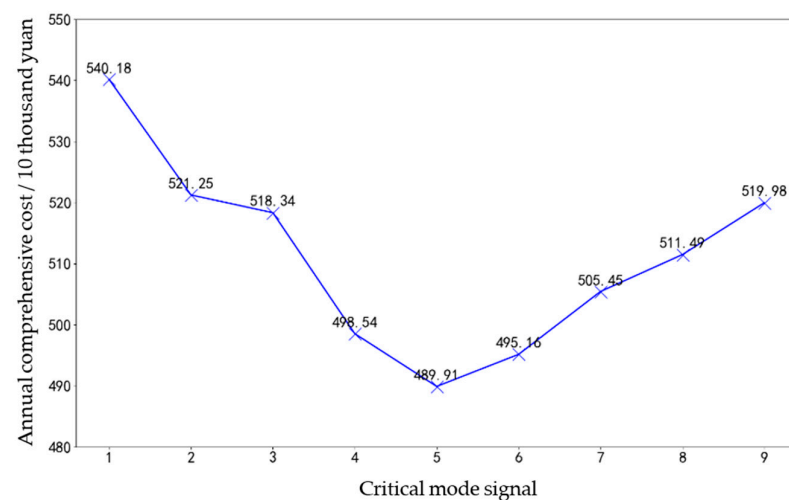


Figure 14. Threshold-annual integrated cost curve.

According to the results of Figure 14, when $m = 5$, that is, the battery storage power command was $P_b = u_1(t) + u_2(t) + u_3(t) + u_4(t)$, the system cost was minimized. Lithium batteries were responsible for the energy storage control of small fluctuations and large amplitude, while the supercapacitors were responsible for the energy storage control of large fluctuations and large amplitude, which matches the technical characteristics of the two types of storage devices, as shown in Figure 15.

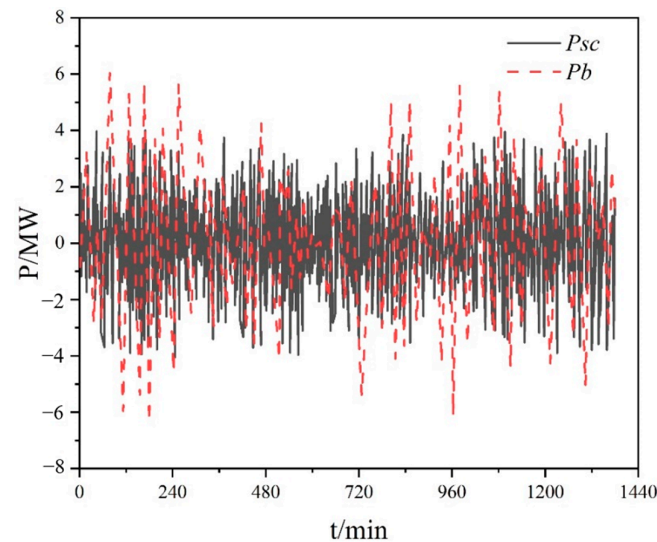


Figure 15. Lithium battery and supercapacitor power curve.

3.3. Quantitative Modeling Analysis of Battery Storage Lifetime

The energy storage cycle of a battery is not only related to the performance of the battery but also to the economic performance of the battery, and the traditional fixed-life model does not consider its variable-life characteristics. This approach does not consider the effects of the scale of the battery energy storage configuration and the charging and discharging states on its life cycle. The power command and rated capacity of the energy storage system will cause different levels of loss in the life cycle of the battery energy storage. The length of the battery storage life cycle determines the number of battery replacements, which will directly affect the comprehensive cost of HESS. In this study, we took lithium-ion batteries as an example and studied the impact of different lifetime models on the annual comprehensive cost of hybrid energy storage systems through the selection of the optimal critical mode. Table 3 lists the annual integrated cost of the hybrid energy storage system under fixed-life model and variable-life model. In the hybrid energy storage system, the annual integrated cost of the energy storage system is inversely related to the life cycle of the lithium-ion battery. As the life cycle increases, fewer batteries need to be replaced during the project period, which reduces the renewal cost. Therefore, the variable-life model for battery storage is more suitable for hybrid energy storage capacity configurations. Different typical days can lead to changes in the quantitative results of the life cycle of battery storage.

Table 3. Lifetime model configuration comparison results.

Life Cycle Model	Fixed-Life Model/a				Variable-Life Model/a
	2	4	6	8	4.1787
$E_B/MW.h$	11.9834	15.8958	18.9863	20.1432	16.6958
P_B/MW	9.1264	9.2579	9.4861	9.4905	9.3423
Cost/million	9.8105	7.3898	6.0318	4.9714	7.4278

3.4. Comparison of Different Energy Storage Schemes

In order to solve the capacity configuration problem of HESS, this study used an event-oriented life model and a rain flow counting method to calculate the cycle times under different discharge depths and analyzed the SOC curve of lithium batteries to calculate the life cycle of battery energy storage. The optimal value of energy storage power command demarcation point was taken as an example to compare the economy of a single-battery and a hybrid energy storage scheme to verify the correctness of the model established in this study, as shown in Table 4.

Table 4. Comparison of different energy storage solutions.

	Lithium Battery	Supercapacitor	Hybrid Energy Storage
$P_B/MW \cdot h$	9.3423	–	5.6876
$E_B/MW \cdot h$	16.6958	–	10.6524
$P_{SC}/MW \cdot h$	–	9.0234	3.8091
$E_{SC}/MW \cdot h$	–	6.541	0.1049
Life/year	4.1787	–	3.9373
Cost/million	7.4278	9.9427	4.8991

A comparison of the combined annual costs of the systems showed that the configuration of a single supercapacitor to undertake the leveling work was the least economical, which was mainly due to the higher capacity cost factor of the supercapacitor. The configuration size of the single-battery energy storage system was much larger than that of the supercapacitor energy storage system, but because of its lower investment cost, the total annual integrated cost decreased by 25.29% relative to the single supercapacitor energy storage system. The hybrid energy storage system combines the complementary technical characteristics of batteries and supercapacitors, and by integrating the cost characteristics of the two to reasonably configure the storage scale, it can effectively reduce the total system cost based on meeting the leveling requirements. As can be seen from the Table 4, the annual comprehensive cost of the hybrid energy storage system decreased by 34.04% relative to the single-battery energy storage system. At the same time, although the battery life in the hybrid energy storage decreased by 5.78% relative to single-battery energy storage, considering the significant decrease in the size of the battery energy storage configuration in hybrid energy storage, especially given its power configuration decreased by 39.12% relative to single-battery energy storage, it can be seen that combining batteries and supercapacitors into a hybrid energy storage system and through a reasonable charging and discharging control strategy can give full play to the complementary advantages of the two and extend the life cycle of battery energy storage.

4. Research on Optimal Allocation of Wind Energy Storage Based on Improved Scenario Clustering Algorithm

In the previous section, a capacity optimization model considering the quantification of the battery life cycle was described for a hybrid energy storage system for smoothing wind power fluctuations, and a cost-optimal configuration of the hybrid energy storage was determined through the optimization solution. Regarding the input data of the energy storage capacity allocation model, i.e., the power command of the energy storage system, as shown in the previous section, a typical day's charging and discharging data of the energy storage system was used instead of the annual charging and discharging data for the capacity allocation model. This alternative can simplify the complexity of the model solution, but the contingency of the selection of a typical day's data will lead to a large deviation of the allocation results from the actual results considering the annual data. If the annual energy storage system charge/discharge data are directly brought into the capacity allocation model, there is the problem of excessive data volume and low computational efficiency. In this study, we considered applying it to the input data processing of the hybrid energy storage capacity optimization allocation model, but the traditional k-means

clustering algorithm has the problems of difficulty in automatically determining the number of clusters and the randomness of the initial clustering center, which will affect the stability and accuracy of the allocation results.

In response to the above problems, in this study, the fuzzy c-means clustering algorithm was applied to hybrid energy storage data processing, which can extract a typical dataset based on the general characteristics of large-scale data; retaining the changing characteristics of the original data also reduces the data volume. To solve the stochastic problem that the existing fuzzy c-means clustering algorithm cannot automatically determine the number of clusters and cluster centers, the hybrid energy storage system constructed in a previous study was used as the object of study, and a new method of selecting the number of clusters and cluster centers to determine the optimal configuration scheme was developed by combining the cloud model and the fuzzy c-means clustering algorithm. Finally, a simulation example was used to verify the stability and accuracy of the configuration results determined according to the algorithm proposed in this section as well as enhancement of the computational accuracy and computational efficiency of the solution process.

4.1. Analysis of Typical Running Curve of Energy Storage Based on Improved Clustering

The set of annual energy storage daily charge and discharge power curves can be divided into two stages: (1) The set of energy storage daily operation curves was obtained according to EEMD decomposition and decomposed into a finite normal cloud model through peak cloud transformation to obtain the initial clustering center. The number of clusters was determined by the frequency limit. (2) According to the initial clustering center and the number of clusters, the fuzzy c-means clustering algorithm was used to aggregate the typical daily charge and discharge curves of 365 days of energy storage.

The flowchart of the improved fuzzy c-means clustering algorithm is shown in Figure 16.

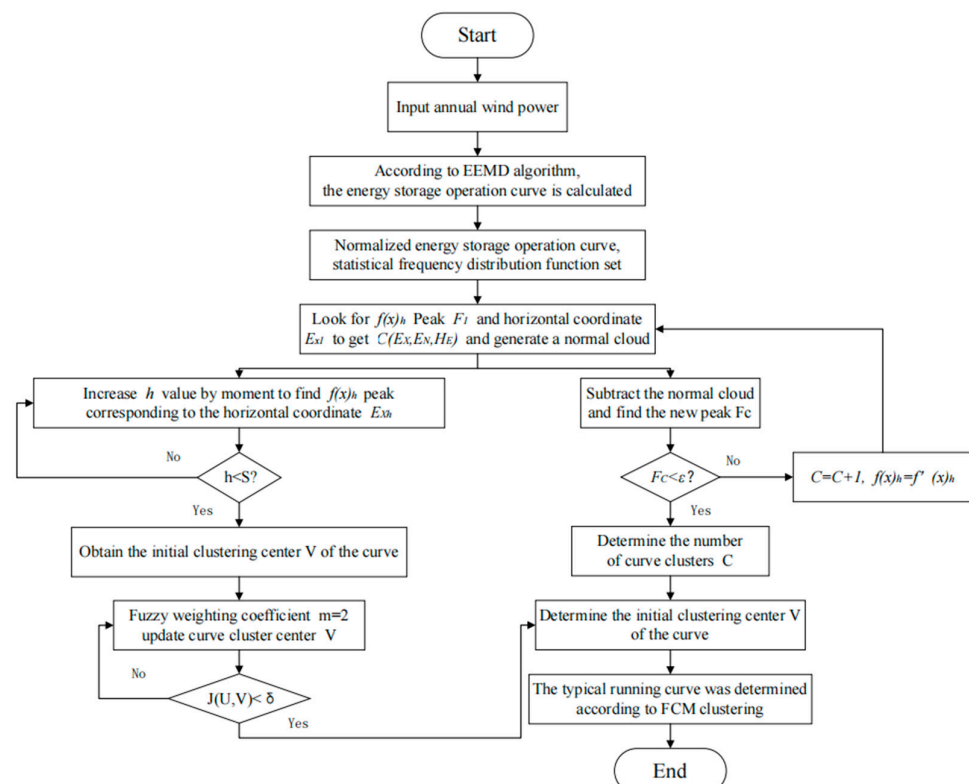


Figure 16. Flowchart of the improved fuzzy c-means algorithm.

In this study, the annual power output data of a 60 MW wind farm was taken as an example, and the annual energy storage operation curve of the energy storage system was

obtained after being flattened by the EEMD decomposition algorithm. The optimal energy storage system configuration scheme was determined by inputting the energy storage capacity optimization model. Figure 17 shows the annual output power of a wind farm, grid-connected power of wind power, and energy storage system power.

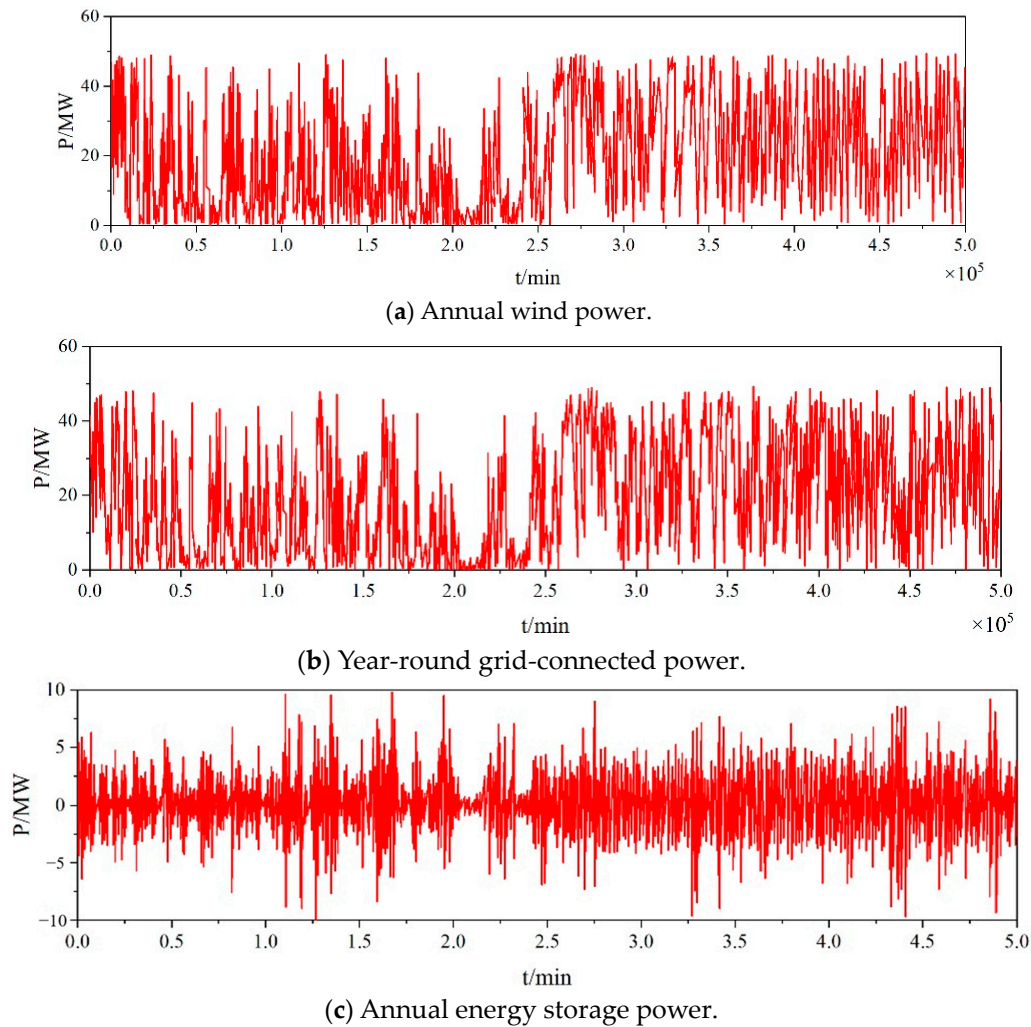


Figure 17. EMD flattening wind power output.

To verify the effectiveness of the analysis of the typical running curve set of energy storage, a single lithium battery energy storage capacity configuration model with a life cycle of 5 years was first selected, and the configuration results of the typical running curve set of energy storage were evaluated to ensure its computational efficiency, accuracy, and stability. Then, it was applied to the capacity optimization configuration of the hybrid energy storage system to further verify its effectiveness.

The battery energy storage system costs were minimized as follows:

$$\min f = C_{Bt} + C_{By} = (k_p P_B + k_e E_B) \frac{r_0(1+r_0)^{T_b}}{(1+r_0)^{T_b} - 1} + k_{py} P_B + k_{ey} E_B \quad (26)$$

where C_{Bt} is the initial investment cost; C_{By} is the annual operation and maintenance cost of the battery; k_p is the power cost coefficient of the battery; k_e is the capacity cost coefficient of the battery; P_B is the rated power of the battery in MW; E_B is the rated capacity, MWh, of the battery; r_0 is the discount rate in percentage; T_b is the operating life of the battery; k_{py} is the power operation and maintenance cost coefficient of the battery; and k_{ey} is the capacity operation and maintenance cost coefficient of the battery.

The constraints on SOC, charge–discharge responsiveness, and energy conservation are as follows:

$$\begin{aligned} SOC_{bmin} &\leq SOC_b(t) \leq SOC_{bmax} \\ \max(-P_B, \frac{E_b(t)-E_B}{\Delta t \eta_{Bc}}) &\leq P_b(t) \leq \min(P_B, \frac{E_b(t)-E_B}{\Delta t} \eta_{Bd}) \\ P_b(t) + P_o(t) &= P_w(t) \end{aligned} \quad (27)$$

where SOC_{bmin} and SOC_{bmax} are the upper and lower limits of the SOC charging state of the battery; $SOC_b(t)$ is the charging state of the battery at time t ; $E_b(t)$ is the remaining power of the battery at time t in MWh; η_{Bc} and η_{Bd} are the charging and discharging efficiencies of the battery, respectively; Δt is the collection frequency in min; $P_b(t)$ is the charging and discharging power of the battery at time t in MW; $P_o(t)$ is the grid-connected power of the wind power at time t after the leveling-off of the hybrid energy storage; and $P_w(t)$ is the original output power of wind power.

When configuring the capacity E_B of the battery energy storage system, the maximum capacity required to ensure the validity of the configuration results is selected:

$$E_B = \max(E_B(1), E_B(2), \dots, E_B(k)) \quad (28)$$

among them,

$$\begin{aligned} E_B(j) &= \max(E_{B1}(j), E_{B2}(j)) \\ E_{B1}(j) &= \max(|\sum_{i=1}^{m_1} P_j \Delta t|, |\sum_{j=m_1}^{m_2} P_j \Delta t|, \dots, |\sum_{j=m_{s-1}}^s P_j \Delta t|) \\ E_{B2}(j) &= \max(|\sum_{j=1}^k P_j \Delta t|), k = 1, 2, \dots, s \end{aligned} \quad (29)$$

where $E_B(j)$ is the capacity required for a single period of time for the j th typical scenario; P_j is the power required for a single period of time for the j th typical scenario; s is the total number of scenarios; and $E_{B1}(j)$ is the capacity required for a single period of time in the j th typical scenario. There are s periods in total, and p is power; $E_{B2}(j)$ indicates the capacity required for the first k period of the j th typical scenario.

4.2. Obtaining the Lithium Battery Energy Storage Configuration Solution

The annual operation curve of energy storage was analyzed by the improved fuzzy c-means algorithm based on the cloud model, and the initial cluster center V and cluster number $k = 8$ were obtained. C and V were input into the fuzzy c-means algorithm as control parameters. The energy storage operation curves of 365 days a year were clustered, and 8 typical daily operation curves were obtained. Table 5 lists the proportions of typical curves.

Table 5. Typical daily curve share.

Typical day	1	2	3	4	5	6	7	8
Proportion/%	38.11	18.19	13.1	4.09	2.6	7.12	1.31	15.36

The typical daily running curve was applied to the above lithium battery energy storage capacity configuration model, and the energy storage power and capacity configuration results were obtained in each typical scenario, as shown in Figures 18 and 19.

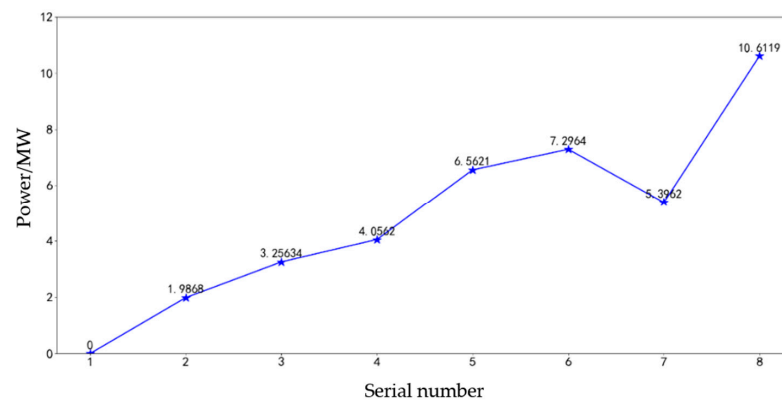


Figure 18. Power requirements for each typical scenario.

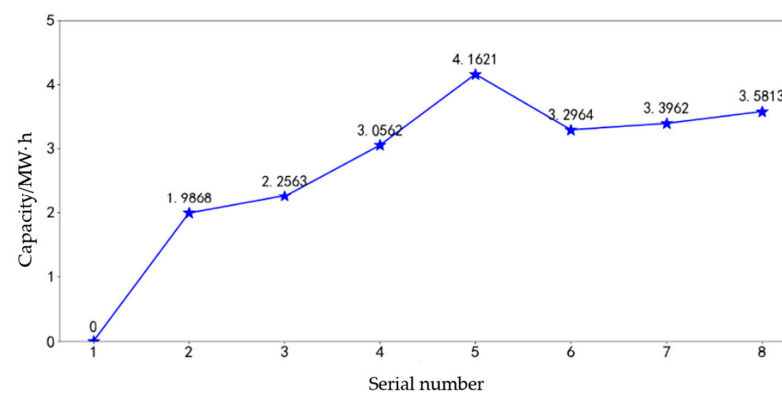


Figure 19. Required capacity for each typical scenario.

It can be seen from the above Figures 18 and 19 that the configuration results of different typical daily curves varied greatly. Therefore, the maximum energy storage capacity and power required should be selected to ensure the effectiveness of the configuration results. The capacity was 4.1621 MWh, the power was 10.6119 MW, and the cost was -RMB 3.7532 million.

4.3. Algorithm Validity Verification Analysis

To verify the effectiveness of the proposed method, the output curve of a wind farm was randomly selected to study, and its energy storage power instruction and energy storage SOC were analyzed. As shown in Figure 20, the grid connection curve showed that its calming effect was good and met the requirements of grid connection.

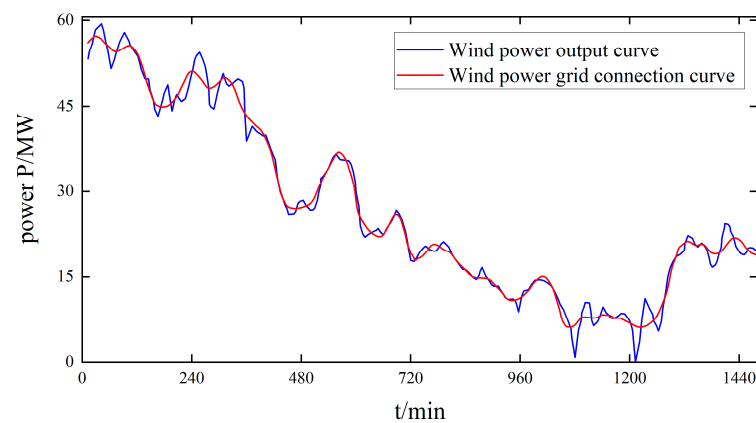


Figure 20. Typical scenario power output and grid connection power curve.

By observing the energy storage power response curve in Figure 21 and the energy storage SOC change curve in Figure 22, it can be seen that the energy storage SOC was always in normal operation. In order to compare the calculation accuracy and efficiency of the energy storage system configuration scheme obtained from different energy storage operation data, the following two data methods were selected as references:

- (1) Typical day method: data of two typical days were randomly selected and input into the lithium battery capacity optimization model.
- (2) Annual timing method: the annual energy storage operation data curve was input into the lithium battery capacity optimization model.

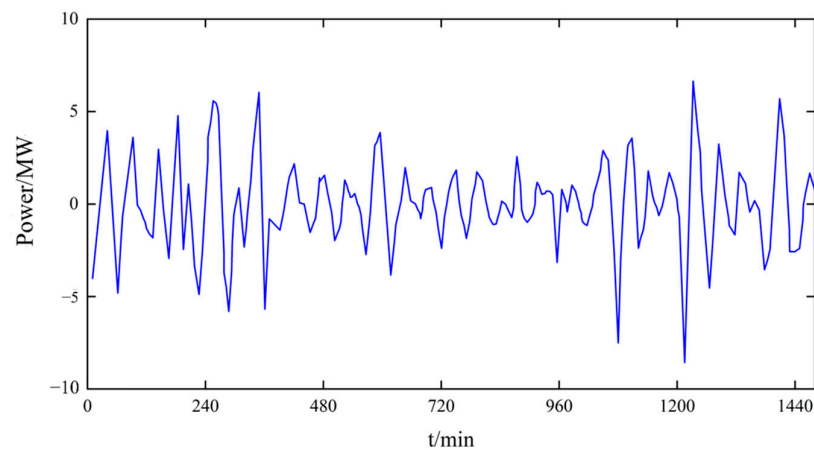


Figure 21. Energy storage power curve.

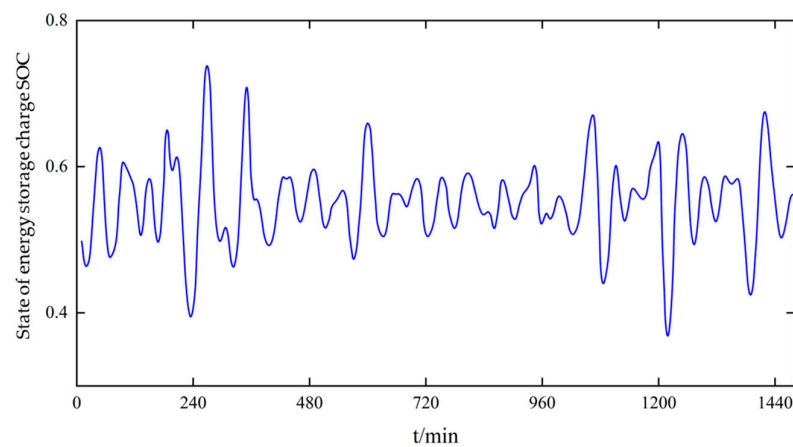


Figure 22. Energy storage SOC curve.

A comparison of the results of the battery energy storage scheme configuration for two randomly selected typical days and the improved clustering method in this paper is shown in Table 6 below.

Table 6. Comparison of different solutions.

	Annual Time Series Data	Typical Day 1	Typical Day 2	Improved Clustering Method
$E_B/MW.h$	4.2678	6.2454	2.7351	4.1621
Capacity error/%	—	46.3	−35.9	−3.6
P_B/MW	10.8302	10.5989	3.6976	10.6119
Power error/%	—	−2.1	−65.9	−2.0
Cost/million	3.8463	4.289	1.7126	3.7532
Cost error/%	—	11.5	−55.5	−2.4
Calculation time/s	1405	12.415	12.501	14.27

It can be seen from Table 6 that compared to standard data, the energy storage configuration scheme calculated by the random typical daily data method had a large error because it was difficult to reflect the change characteristics of the annual operating curve with typical daily data. The capacity error, power error, and cost error of the proposed algorithm were all about 3%. The calculation time was also significantly reduced compared to the annual time series simulation, and the calculation efficiency was greatly improved.

4.4. Stability Analysis of Initial Cluster Center

In order to verify the superiority of the improved clustering algorithm, 10 classical fuzzy c-means clustering experiments were conducted, in which the initial clustering centers were randomly selected and the number of clusters was given as $k = 8$. The method of automatically determining the number of clusters and initial clustering centers using the cloud model can effectively avoid problems such as poor stability of results and easily falling into local optimal solutions. Table 7 describes the configuration structure.

Table 7. Comparison of the mean values of 10 experiments with the improved clustering method.

	Annual Time Series Data	The Mean of Ten Experiments	Improved Clustering Method
$E_B/MW \cdot h$	4.2678	4.5683	4.1621
Capacity error/%	—	7.0	−3.6
P_B/MW	10.8302	10.4682	10.6119
Power error/%	—	−3.3	−2.0
Cost/million	3.8463	3.7126	3.7532
Cost error/%	—	−3.5	−2.4
Single calculation time/s	1405	15.52	14.27

By comparing the mean experiment with the algorithm, it was found that a large number of experimental means could improve the configuration bias to a certain extent. However, compared to the improved clustering algorithm, there was no obvious advantage in the result accuracy. In addition, while the number of clusters was the same, the calculation time of the traditional fuzzy c-means algorithm was not much different from that of the proposed algorithm in a single experiment. However, when the experiment was repeated 10 times and the average was taken, the computational efficiency was significantly reduced.

4.5. Rationality Analysis of the Number of Automatic Clustering

In order to verify the rationality of the improved clustering algorithm to automatically determine the number of clusters, the mean results of the experimental processing of energy storage operation curve configuration by repeating the traditional fuzzy c-means algorithm under different cluster numbers were selected for comparison, and the comparison results are shown in Table 8.

Table 8. Comparison of the number of different clusters.

	Annual Timing	C = 3	C = 6	C = 9	C = 15	Improved Clustering Method
$E_B/MW \cdot h$	4.2678	3.7091	4.1235	4.4819	4.2053	4.1621
Capacity error/%	—	−13.3	−3.4	5.0	−1.5	−3.6
P_B/MW	10.8302	9.6205	10.5618	10.9635	11.0516	10.6119
Power error/%	—	−11.2	−2.5	1.2	2.1	−2.0
Cost/million	3.8463	3.3524	3.7356	3.9215	3.8109	3.7532
Cost error/%	—	−12.8	−2.9	2.0	1.2	−2.4
Single calculation time/s	1405	13.35	15.15	16.36	29.03	14.27

The configuration error caused by the traditional fuzzy c-means algorithm decreased gradually with the increase in the number of clusters, but the calculation time also increased

gradually. When the number of clusters was similar, the number of clusters of the traditional fuzzy c-means algorithm and the improved clustering algorithm were similar, the error was basically the same, and the single calculation time was similar. When the number of clusters was further increased to a large size, the error was only slightly reduced, but the single calculation time was greatly increased, and the calculation time of repeated experiments was very large. In summary, the improved clustering algorithm can improve the computational efficiency of the configuration process and ensure reasonable error of the configuration results.

4.6. Comparison of Hybrid Energy Storage Configuration Schemes

According to the above analysis and verification for a single lithium battery, the improved clustering algorithm based on the cloud model can improve the sensitivity of cluster center selection and the randomness of artificially determining the number of clusters in the traditional fuzzy c-means algorithm when dealing with the energy storage running curve, thus improving the stability and accuracy of capacity configuration. Next, we studied the hybrid energy storage capacity configuration.

Using the internal power instruction distribution method of the energy storage system, the typical operation curve set of energy storage obtained by the improved fuzzy c-means clustering method based on the cloud model was decomposed into lithium battery power instruction and supercapacitor power instruction, which were input into the hybrid energy storage capacity configuration model outlined in the previous section.

The objective function was to minimize the cost of the energy storage system:

$$\begin{aligned} \min f = C_B^* + C_{SC}^* = & (k_p P_B + k_e E_B) \frac{r_0(1+r_0)^{T_b}}{(1+r_0)^{T_b}-1} + \\ & k_{py} P_B + k_{eg} E_B + \sum_{i=1}^n (k_{pg} P_B + k_e E_B) (1+r_0)^{\frac{iT_b}{n+1}} + \\ & + (\lambda_p P_{SC} + \lambda_e E_{SC}) \frac{r_0(1+r_0)^{T_{sc}}}{(1+r_0)^{T_{sc}}-1} + \lambda_{py} P_{SC} + \lambda_{ey} E_{SC} \end{aligned} \quad (30)$$

where f is the annual comprehensive cost of the hybrid energy storage system; C_B^* is the annual comprehensive cost of battery energy storage; C_{SC}^* is the annual comprehensive cost of supercapacitor energy storage; n is the number of times of battery renewal and replacement; T_{sc}/T_b is determined by the service life of the battery, T_b , and the set life of the supercapacitor, T_{sc} ; k_{pg} is the cost coefficient of the power renewal of the battery; T_{sc} is the operating life of the supercapacitor; P_{SC} is the rated power of the supercapacitor in MW; E_{SC} is the rated capacity of the supercapacitor in MW; λ_p , λ_e , λ_{py} , and λ_{ey} are the power cost coefficient, capacity cost coefficient, power operation and maintenance cost coefficient, and capacity operation and maintenance cost coefficient of the supercapacitor, respectively.

The decomposed power instruction set was substituted into the capacity optimization model of the hybrid energy storage system, and the results of the randomly selected typical daily data method and improved clustering method were compared with the annual time series method.

According to the observation results in Table 9, it can be seen that the annual time series data method required a large amount of data and had low calculation efficiency. However, the random selection of typical daily data could not accurately reflect the changing characteristics of the annual running curve, resulting in a large error in the configuration scheme. In contrast, the data processing method proposed in this paper could not only greatly improve the computational efficiency but also control the capacity error, power error, and cost error within an acceptable range.

Table 9. Hybrid energy storage solution results.

	Annual Time Series Data	Typical Day 1	Typical Day 2	Improved Clustering Method
$E_B/MW \cdot h$	2.8419	4.0725	3.3015	3.0235
Capacity error/%	—	43.3	16.2	6.4
P_B/MW	7.2142	11.0651	5.3645	7.4384
Power error/%	—	53.4	−25.6	3.1
$E_{SC}/MW \cdot h$	0.2135	0.2446	0.2245	0.2045
Capacity error/%	—	14.5	5.2	−4.2
P_{SC}/MW	4.2546	3.7548	4.7862	4.0564
Power error/%	—	−11.7	12.5	−4.7
cost/million	3.1645	3.3546	4.9454	3.0453
cost error/%	—	6.0	56.3	−3.8
calculation time/s	2265	17.58	16.82	24.96

The experimental results showed that the proposed method could automatically determine the number of clusters and the initial cluster center, avoid the sensitivity problem of randomly given cluster number and the initial cluster center, and effectively improve the stability and accuracy of the configuration results.

5. Conclusions

The results of this study enrich the theoretical system and technical architecture in the research field of grid-connected wind farm side hybrid energy storage systems and provide new solution ideas and technical references for improving the quality of wind power grid connection, thus optimizing the effect of hybrid energy storage management, perfecting the capacity optimization model of hybrid energy storage systems, and improving the solving accuracy and efficiency of the energy storage optimization model. The main results of this paper are summarized as follows:

- (1) According to the different characteristics of energy storage technology, the charging and discharging response frequency characteristics and charging and discharging response capability of various energy storage units were analyzed and compared, and the lithium-ion battery supercapacitor was selected to develop a hybrid energy storage system that breaks through the limitations of single energy storage technology and, at the same time, has the advantages of both energy-type and power-type energy storage systems. The principle of wind power generation was explained, the output factors were analyzed, the quantitative mathematical model of output was examined, the time-frequency domain characteristics of wind power output was studied, and a foundation was laid for subsequent capacity allocation and economic evaluation under the wave smoothing scenario.
- (2) The EEMD algorithm was used for the smoothing decomposition of raw wind power data, which was a random perturbation added to EMD in order to solve the problems of model aliasing and slow convergence in EMD. Wind power grid-connected power and energy storage power data were extracted according to China's wind power grid-connected fluctuation standard combined with EEMD's decomposition and reconstruction of wind power. The simulation results showed that EEMD decomposition could adapt to the fluctuation power smoothing of different wind power output scenarios, and its smoothing effect was better than that of the low-pass filtering algorithm. For the allocation of power inside the hybrid energy storage system, this study adopted the method of primary allocation and secondary fuzzy correction based on response characteristics to obtain the storage power commands of Li-ion batteries and supercapacitors. The primary allocation was mainly considered to reduce the influence of the charging and discharging response frequency of Li-ion batteries' energy storage to its life cycle, and the secondary correction was based on the fuzzy control of the hybrid storage SOC, which realized reasonable allocation of the power commands of the hybrid energy storage, improved the safety of the storage system, and ensured improvement of the regulation characteristics and the

operation economy of the hybrid energy storage system. (3) The capacity allocation model of the energy storage system considering the life cycle cost was established, and the number of cycles corresponding to the charging and discharging depths was counted using the rainfall counting method to derive the life cycle of the battery energy storage. The capacity allocation model for lithium battery storage, the capacity allocation model for supercapacitor storage, and the capacity allocation model for hybrid storage were established. By comparing different power distribution dividing points of the hybrid energy storage system and their corresponding comprehensive costs, the optimal dividing point was selected. Finally, the optimal critical modes were determined by exhaustively enumerating the demarcation points of different high- and low-frequency bands. The different energy storage configuration schemes were also compared and analyzed. The simulation results showed that the proposed method had certain economic and technical advantages.

- (3) A combination of the cloud model and fuzzy c-means algorithm was applied to study the capacity allocation of wind energy storage systems. Feature extraction and scene division were used for the annual storage daily power curve, which was conducive in simplifying the calculation. The analysis of energy storage operation curve based on cloud model theory can reasonably determine the number of clusters and the initial clustering center of fuzzy c-means algorithm, which overcomes the shortcomings of traditional fuzzy c-means that needs to artificially give the number of clusters and the initial clustering center randomly, and the application of it in capacity optimization also enhances the stability and accuracy of the configuration results. After clustering analysis, eight classes of typical operating curves were obtained and input into the hybrid energy storage system capacity optimization model. Simulation analysis showed that the number of clusters and the initial cluster centers automatically determined by the cloud model could avoid the irrationality caused by randomly given cluster numbers and the defects of sensitivity of the initial cluster centers, thus effectively improving the stability and accuracy of the configuration results. This proves that the combination of the cloud model theory and fuzzy c-means can achieve better results when studying wind energy storage capacity configuration.

The research outlined in this paper focused on the control strategy of energy storage in smoothing the power fluctuation of wind farms on the grid and the allocation of energy storage capacity. However, due to the authors' limited knowledge and research time, there are still many deficiencies and areas for improvement as well as many issues and directions worthy of further research:

- (1) In this study, only direct grid connection to meet the wind power grid connection standard was considered. However, in actual operation, there are complex factors at play, such as the impact of power load changes on the grid-connected power of wind farms, the adjustment of peak and valley tariff differences on the grid-connected power of wind farms, and frequency-assisted control of the power system. In the next step of the study, the impact of these factors on grid-connected power will be considered, and the control strategy and energy storage capacity allocation method will be further optimized.
- (2) The study of leveling based on historical data of wind power generation lacks in-depth research on the issues of response delay and cannot control wind power leveling on-line in real time. The future research direction should be to realize wind power leveling through real-time control in order to improve the real-time nature of the control strategy during leveling.
- (3) In constructing the cost model of the hybrid energy storage system, the influence of other aspects of wind power systems, such as energy saving and emission reduction, were not taken into account. Therefore, in future research, the above influences can be introduced into the cost model of hybrid energy storage systems to construct a better cost model.

- (4) The function of hybrid energy storage systems on the wind farm side is not only limited to suppressing wind power fluctuations and also plays an important role in regulating the planned output of wind power, assisting the power system frequency control, supporting the stability of reactive power in wind farms, and enhancing the fault ride-through capability of wind turbines. Subsequent research can consider combining different control objectives for complex control, adjusting the active and reactive power outputs of the hybrid energy storage system according to the control needs of wind farms and power grids in different operating states, and improving the power supply adequacy and operational stability of connected large-scale wind power systems.
- (5) Based on the economic and technical characteristics of the current energy storage materials, this study selected batteries and supercapacitors to form a hybrid energy storage system. Considering that the research of advanced energy storage materials is a hotspot and there is a great possibility of key breakthroughs in the future, subsequent research needs to pay attention to the progress being made on the research of advanced energy storage materials. This includes tracking the development of energy storage materials, adjusting the hybrid storage combination mode in a timely manner, and improving the energy storage control strategy and the configuration model accordingly.

Author Contributions: Conceptualization, J.Z. and P.C.; writing—original draft preparation, T.Z.; writing—revision, T.Z.; supervision, J.Z. and P.C.; formal analysis D.Y. and X.T.; project administration, J.Z. and J.Y.; All authors have read and agreed to the published version of the manuscript.

Funding: This work was supported in part by the National Key Research and Development Program Project (Grant number: 2019YFE0104800) and Scientific and Technological Research Project of Henan Provincial Department of Education (Grant number: 20A210027). This work was supported in part by the Scientific and Technological Innovation Team of Colleges and Universities in Henan Province under Grant 22IRTSTHN011.

Data Availability Statement: Data are contained within the article.

Conflicts of Interest: The authors declare no conflict of interest.

References

- Ren, J.; Chen, D.Z.; Song, Y.T.; Wang, B.N.; Tian, J.S. Analysis of the impact of large-scale wind power access on system frequency characteristics. *Power Technol.* **2016**, *40*, 1491–1494.
- Xiaoming, Y.; Shijie, C.; Jinyu, W. Prospect analysis of the application of energy storage technology in solving the problem of large-scale wind power grid integration. *Power Syst. Autom.* **2013**, *37*, 14–18.
- Li, X.J.; Yao, L.Z.; Hui, D. Optimal control and management of a large-scale battery energy storage system to mitigate fluctuation and intermittence of renewable generations. *J. Mod. Power Syst. Clean Energy* **2016**, *4*, 593–603. [\[CrossRef\]](#)
- Faheem, M.; Umar, M.; Butt, R.A.; Raza, B.; Ngadi, M.A.; Gungor, V.C. Software Defined Communication Framework for Smart Grid to Meet Energy Demands in Smart Cities. In Proceedings of the 2019 7th International Istanbul Smart Grids and Cities Congress and Fair (ICSG), Istanbul, Turkey, 25–26 April 2019; pp. 51–55. [\[CrossRef\]](#)
- Faheem, M.; Butt, R.A. Big datasets of optical-wireless cyber-physical systems for optimizing manufacturing services in the internet of things-enabled industry 4.0. *Data Brief* **2022**, *42*, 108026. [\[CrossRef\]](#) [\[PubMed\]](#)
- Chemali, E.; Preindl, M.; Malysz, P.; Emadi, A. Electrochemical and Electrostatic Energy Storage and Management Systems for Electric Drive Vehicles: State-of-the-Art Review and Future Trends. *IEEE J. Emerg. Sel. Top. Power Electron.* **2016**, *4*, 1117–1134. [\[CrossRef\]](#)
- Wang, C.-N.; Yang, F.-C.; Vo, N.T.M.; Nguyen, V.T.T. Enhancing Lithium-Ion Battery Manufacturing Efficiency: A Comparative Analysis Using DEA Malmquist and Epsilon-Based Measures. *Batteries* **2023**, *9*, 317. [\[CrossRef\]](#)
- Zhao, H.; Wang, X.; Li, B.; Si, Q.; Zhao, M. Distributionally Robust Optimal Dispatch for Multi-community Photovoltaic and Energy Storage System Considering Energy Sharing. *Autom. Electr. Power Syst.* **2022**, *46*, 21–31. [\[CrossRef\]](#)
- Fortenbacher, P.; Mathieu, J.L.; Andersson, G. Modeling and optimal operation of distributed battery storage in low voltage grids. *IEEE Trans. Power Syst.* **2017**, *32*, 4340–4350. [\[CrossRef\]](#)
- Sakti, A.; Gallagher, K.G.; Sepulveda, N.; Uckun, C.; Vergara, C.; de Sisternes, F.J.; Dees, D.W.; Botterud, A. Enhanced representations of lithium-ion batteries in power systems models and their effect on the valuation of energy arbitrage applications. *J. Power Sources* **2017**, *342*, 279–291. [\[CrossRef\]](#)

11. Guo, T.; Liu, Y.; Zhao, J.; Zhu, Y.; Liu, J. A Dynamic Wavelet-based Robust Wind Power Smoothing Approach Using Hybrid Energy Storage System. *Int. J. Electr. Power Energy Syst.* **2020**, *116*, 105579. [\[CrossRef\]](#)
12. Chao, C.; Yuxin, M.; Yue, C.; Ruifeng, G. Hybrid energy storage capacity allocation method based on empirical modal decomposition and fuzzy chance constraint. *Distrib. Energy* **2016**, *1*, 43–48.
13. Zhang, J.; Hu, Y. Optimization Strategy for Hybrid Energy Storage Power Distribution Based on Fuzzy Control. *J. Phys. Conf. Ser.* **2020**, *1549*, 052115. [\[CrossRef\]](#)
14. Santhosh, M.; Venkaiah, C.; Kumar, D.V. Ensemble Empirical Mode Decomposition based Adaptive Wavelet Neural Network Method for Wind Speed Prediction. *Energy Convers. Manag.* **2018**, *168*, 482–493. [\[CrossRef\]](#)
15. Chen, L.; Wang, J.; Sun, Z.; Huang, T.; Wu, F. Smoothing Photovoltaic Power Fluctuations for Cascade Hydro-PV-pumped Storage Generation System Based on a Fuzzy CEEMDAN. *IEEE Access* **2019**, *7*, 172718–172727. [\[CrossRef\]](#)
16. Sun, S.; Fu, J.; Wei, L.; Li, A. Multi-Objective Optimal Dispatching for A Grid-Connected Micro-Grid Considering Wind Power Forecasting Probability. *IEEE Access* **2020**, *8*, 46981–46997. [\[CrossRef\]](#)
17. Lu, J.; Zhang, W.; Zhang, X.; Wang, B.N.; Tian, J.S. Coordinated control strategy for photovoltaic micro-grid system with hybrid energy-storage. *Power CSUEPSA* **2021**, *33*, 102–108.
18. Baker, K.; Gabriela, H.; Xin, L. Energy storage sizing taking into account forecast uncertainties and receding horizon operation. *IEEE Trans. Sustain. Energy* **2017**, *8*, 331–340. [\[CrossRef\]](#)
19. Deng, Z.; Xu, Y.; Gu, W.; Fei, Z. Finite-time convergence robust control of battery energy storage system to mitigate wind power fluctuations. *Int. J. Electr. Power Energy Syst.* **2017**, *91*, 144–154. [\[CrossRef\]](#)
20. Zhang, Q.; Li, X.; Yang, M.; Cao, Y.; Li, P. Hybrid energy storage capacity allocation method for smoothing wind power fluctuations with maximum net benefit. *J. Electrotechnol.* **2016**, *31*, 40–48.
21. Liu, Y.M.; Wang, X.D.; Peng, C.H. A predictive control strategy for smoothing wind power model taking into account the storage output level. *Grid Technol.* **2020**, *44*, 1723–1731.
22. Lamsal, D.; Sreeram, V.; Mishra, Y.; Kumar, D. Smoothing control strategy of wind and photovoltaic output power fluctuation by considering the state of health of battery energy storage system. *IET Renew. Power Gener.* **2019**, *13*, 578–586. [\[CrossRef\]](#)
23. Yilin, Y.; Suhua, L.; Yaowu, W.; Yangtian, M. Optimisation of battery storage capacity for improving wind power dispatchability based on variable life model. *J. Electrotechnol.* **2015**, *30*, 53–59.
24. Zhang, F.; Liang, J.; Zhang, L.; Han, X.; Wang, H.; Wei, K. Optimisation method of wind farm energy storage capacity considering optimal desired output and charge state. *Power Syst. Autom.* **2014**, *38*, 12–19.
25. Chengchen, S.; Yue, Y.; San Shing, O.I.; Mengting, L.; Xinsong, Z.; Yang, C. Optimal allocation of hybrid energy storage capacity for microgrids based on empirical modal decomposition and neural network. *Power Syst. Autom.* **2015**, *39*, 19–26.
26. Savkin, A.V.; Khalid, M.; Agelidis, V.G. A constrained monotonic charging/discharging strategy for optimal capacity of battery energy storage supporting wind farms. *IEEE Trans. Sustain. Energy* **2016**, *7*, 1224–1231. [\[CrossRef\]](#)
27. Han, X.; Ji, T.; Li, B. Mining typical operating curves of energy storage systems under defined application scenarios. *Chin. J. Electr. Eng.* **2016**, *36*, 978–985.
28. Wu, T.; Shi, X.; Liao, L.; Zhou, C.; Zhou, H.; Su, Y. A Capacity Configuration Control Strategy to Alleviate Power Fluctuation of Hybrid Energy Storage System Based on Improved Particle Swarm Optimization. *Energies* **2019**, *12*, 3498. [\[CrossRef\]](#)
29. Wang, R.; Shang, H. Application of improved fuzzy decision-making in the evaluation of wind power industry. *J. North China Inst. Water Conserv. Hydropower* **2012**, *33*, 59–61.
30. Zou, M.K.; Dai, B.R.; Peng, C.; Xin, X.S.; Luo, W.Q. A hybrid energy storage wind power levelling method based on hierarchical optimization of charge state. *Power Syst. Autom.* **2013**, *37*, 1–6.
31. Li, F.; Xie, K.; Zhang, X.; Wang, K.; Zhou, D.; Zhao, B. Design of control strategy for hybrid energy storage system based on lithium battery charging and discharging states. *Power Syst. Autom.* **2013**, *37*, 70–75.
32. Han, X.; Chen, Y.; Zhang, H.; Chen, F. Application of hybrid energy storage technology based on wavelet packet decomposition in smoothing power fluctuation of wind farm. *Chin. J. Electr. Eng.* **2013**, *33*, 8–13.
33. Chaoxian, L.; Xinran, L.; Longhui, T.; Li, Y.; Jing, H. Smoothing strategy for multi-type energy storage system based on wavelet frequency division and two-layer fuzzy control. *Power Syst. Autom.* **2015**, *39*, 21–29.
34. Xiong, X.; Wang, J.; Yang, R.; Ye, L. Fuzzy adaptive control strategy for hybrid energy storage in microgrid. *Grid Technol.* **2015**, *39*, 677–681.
35. Zhao, H.; Wu, Q.; Wang, C.; Cheng, L.; Rasmussen, C.N. Fuzzy logic based coordinated control of battery energy storage system and dispatchable distributed generation for microgrid. *J. Mod. Power Syst. Clean Energy* **2015**, *3*, 422–428. [\[CrossRef\]](#)
36. Ke, D.; Chung, C.Y. Design of Probabilistically-Robust Wide-Area Power System Stabilizers to Suppress Inter-Area Oscillations of Wind Integrated Power Systems. *IEEE Trans. Power Syst.* **2016**, *31*, 4297–4309. [\[CrossRef\]](#)
37. Yuming, C.; Peng, J.; Gaojun, M.; Yao, W.; Tiantian, L. Optimal Capacity Configuration of Hybrid Energy Storage System Considering Smoothing Wind Power Fluctuations and Economy. *IEEE Access* **2022**, *10*, 101229–101236. [\[CrossRef\]](#)

38. Ghelardoni, L.; Ghio, A.; Anguita, D. Energy Load Forecasting Using Empirical Mode Decomposition and Support Vector Regression. *IEEE Trans. Smart Grid* **2013**, *4*, 549–556. [[CrossRef](#)]
39. Tran, V.T.; Le, M.H.; Vo, M.T.; Le, Q.T.; Hoang, V.H.; Tran, N.T.; Nguyen, V.T.; Nguyen, T.A.T.; Nguyen, H.N.; Nguyen, V.T.T.; et al. Optimization design for die-sinking EDM process parameters employing effective intelligent method. *Cogent Eng.* **2023**, *10*, 2264060. [[CrossRef](#)]

Disclaimer/Publisher’s Note: The statements, opinions and data contained in all publications are solely those of the individual author(s) and contributor(s) and not of MDPI and/or the editor(s). MDPI and/or the editor(s) disclaim responsibility for any injury to people or property resulting from any ideas, methods, instructions or products referred to in the content.